New Semidefinite Programming Joint Localization and Synchronization Using Sequential One-Way TOAs and Doppler Shifts

Yanyan Peng, Ningyan Guo, Sihao Zhao, *Senior Member, IEEE*, Chunxiao Jiang, *Fellow, IEEE*, and Zhiyong Feng, *Senior Member, IEEE*

***Abstract*—In a time-division (TD) broadcast localization and synchronization (TDBLAS) system, moving user nodes (UNs) with the clock offset and the clock drift usually use the sequential one-way time-of-arrival (TOA) and Doppler shift measurements from the anchor nodes (ANs) to resolve the joint localization and synchronization (JLAS) problem in the presence of the AN position error. The objective function of the maximum likelihood (ML) method to solve the above JLAS problem in a TDBLAS system is high-dimensional nonlinear and nonconvex. Thus, the existing iterative method for solving the above ML estimation problem usually encounters issues like local minima or nonconvergence when an accurate initial guess is missing. In this article, we propose a new semidefinite programming (SDP) method to address this issue, which can guarantee the global optimal solution without requiring initialization. We introduce the optimization variable and formulate a nonconvex-constrained weighted least-squares (CWLS) minimization problem. Subsequently, we propose a novel semidefinite relaxation (SDR) approach to relax the complex and nonconvex CWLS problem into a convex and tractable SDP problem. Through theoretical estimation error analysis, we demonstrate that the CWLS solution can achieve the Cramér–Rao lower bound (CRLB) under small Gaussian noise. Simulation results in a 2-D scenario show that the proposed SDP method reaches the CRLB under small Gaussian noise. Compared to the conventional iterative method, the proposed SDP method exhibits greater robustness, achieving the global optima without requiring initialization under small Gaussian noise.**

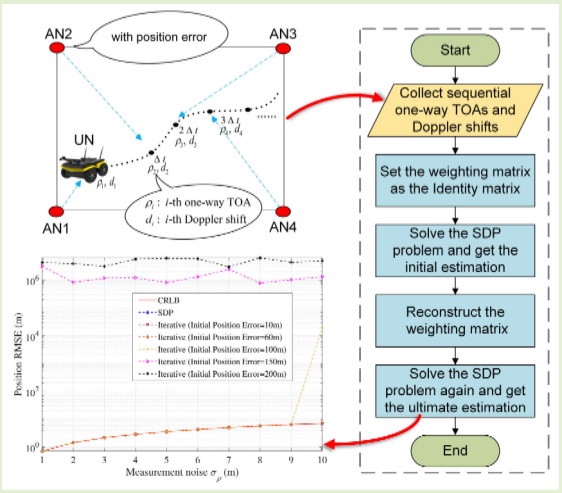

***Index Terms*— Anchor node (AN) position error, Doppler shift, joint localization and synchronization (JLAS), moving user node (UN), semidefinite programming (SDP), time of arrival (TOA).**

NOMENCLATURE

x	Scalar.
$\boldsymbol{x}$	Vector.
$\boldsymbol{X}$	Matrix.

Received 6 March 2025; accepted 11 April 2025. Date of publication 21 April 2025; date of current version 2 June 2025. This work was supported in part by the National Natural Science Foundation of China under Grant 62321001 and Grant 62103226. The associate editor coordinating the review of this article and approving it for publication was Dr. Ing. Ni Zhu. *(Corresponding authors: Ningyan Guo; Sihao Zhao.)*

Yanyan Peng, Ningyan Guo, and Zhiyong Feng are with the Key Laboratory of Universal Wireless Communications, Ministry of Education, Beijing University of Posts and Telecommunications, Beijing 100876, China (e-mail: pengyanyan@bupt.edu.cn; guoningyan@bupt.edu.cn; fengzy@bupt.edu.cn).

Sihao Zhao is with NovAtel, Autonomy and Positioning Division of Hexagon, Calgary, AB T3K 2L5, Canada (e-mail: zsh01@tsinghua.org.cn).

Chunxiao Jiang is with the Tsinghua Space Center, Tsinghua University, Beijing 100084, China (e-mail: jchx@tsinghua.edu.cn).

Digital Object Identifier 10.1109/JSEN.2025.3560989

$\hat{x}$, $\hat{\boldsymbol{x}}$	Estimate of a variable.
$\|\boldsymbol{x}\|$	Euclidean norm of a vector.
$\boldsymbol{X}^T$	Transpose of a matrix.
$\boldsymbol{X}^{-1}$	Inverse of a matrix.
$\text{rank}(\boldsymbol{X})$	Rank of a matrix.
$\text{tr}(\boldsymbol{X})$	Trace of a matrix.
$\|\boldsymbol{X}\|$	Determinant of a matrix.
$[\boldsymbol{X}]_{u,:}$, $[\boldsymbol{X}]_{:,v}$	uth row and the vth column of a matrix, respectively.
$[\boldsymbol{X}]_{u:v,m:n}$	Submatrix with the uth to the vth rows and the mth to the nth columns.
$[\boldsymbol{X}]_{u,v}$	Entry at the uth row and the vth column of a matrix.
$[\boldsymbol{x}]_{u:v}$	Subvector with the uth to the vth elements.
$[\boldsymbol{x}]_u$	uth element of a vector.

$\mathbf{0}_N$, $\mathbf{1}_N$	N-element vectors consisting of all zeros and ones.
$\mathbb{E}[\cdot]$	Expectation operator.
$\boldsymbol{A} \succeq \mathbf{0}$	Matrix $\boldsymbol{A}$ is positive semidefinite.
diag$\{\cdot\}$	Diagonal matrix with the elements along the main diagonal.
M	Number of ANs.
K	Dimensions of all the position and velocity vectors, that is, $K = 2$ in 2-D cases and $K = 3$ in 3-D cases.
i, j	Index of the measurement.
$(\cdot)^o$	True value.
$(\cdot)$	Noisy value.
ρ_i	One-way TOA measurement between the UN and the AN #i.
d_i	Doppler shift measurement between the UN and the AN #i.
$\boldsymbol{q}_i$	Known position vector of the AN #i.
$\boldsymbol{p}$, $\boldsymbol{v}$	Unknown position and velocity vectors of the UN.
ζ, ω	Unknown clock offset and clock drift between UNs and ANs.
Δt, Δt_i	Time intervals between successive measurements, and $\Delta t_i = \Delta t \cdot (i-1)$.
ε, σ^2	Gaussian measurement noise and variance.
$\boldsymbol{\Sigma}_\rho$, $\boldsymbol{\Sigma}_d$	Variance matrices of one-way TOAs and Doppler shift noises.
$\boldsymbol{\theta}$	Parameter vector.
$\boldsymbol{W}$	Weighting matrix.
$\boldsymbol{y}$	Optimization variable.
$\boldsymbol{Y}$	Matrix related to the optimization variable $\boldsymbol{y}$.
m	Rank of matrix $\boldsymbol{Y}$.
n	Number of equality constraints of the standard SDP problem.
$\mathcal{F}$	Fisher information matrix.
$\boldsymbol{e}_i$	Unit line-of-sight (LOS) vector from the UN to the AN #i.
α, β, and μ	Magnitude values related to the initial value of the weighting matrix $\boldsymbol{R}^{-1}$.

I. Introduction

JOINT localization and synchronization (JLAS) systems have attracted significant attention over the past few decades, playing a crucial role in numerous practical applications, such as Internet of Vehicles (IoVs), aerial surveillance, emergency rescue, and target detection and tracking [1], [2], [3], [4]. Typically, such systems consist of multiple synchronous anchor nodes (ANs) located at known positions and mobile user nodes (UNs) with unknown positions and the clock offset that require localization and synchronization. In general, time of arrival (TOA), time difference of arrival (TDOA), received signal strength (RSS), angle of arrival (AOA), and their combinations are the most commonly used measurements that provide range and timing information between ANs and UNs [5], [6], [7], [8], [9], [10], [11], [12], [13], [14], [15]. Notably, TOA measurement is widely preferred in real-world applications due to its simplicity and high accuracy [16], [17], [18], [19], [20], [21]. Furthermore, Doppler shift measurements become important when there exists relative motion between ANs and UNs. Doppler shift measurements can be combined with TOA measurements to estimate moving UNs' velocities and the clock drifts, which can improve the estimation accuracy of UNs' positions [22], [23], [24], [25], [26].

Recent studies have combined the TOA and Doppler shift measurements for the JLAS problem. The work in [22] studies the localization of the moving object using the maximum likelihood estimators (MLEs) in the presence of the sensors' motion. The research in [23] introduces a two-step nonlinear weighted least-squares (WLS) technique, offering a global optimum for the estimation of the unknown UNs' positions and velocities. In [24], an algebraic closed-form solution is introduced for the moving target localization which can reach the Cramér–Rao lower bound (CRLB) under small Gaussian noise. The method proposed in [25] is based on multidimensional scaling (MDS) for the moving target localization, which is robust to large measurement errors. The study in [26] proposes a semidefinite relaxation (SDR) method to estimate the moving object's position and velocity. However, these studies are based on the concurrent TOA and Doppler shift measurements, which do not apply to the time-division (TD) broadcast systems [27], [28], [29], where sequential measurements are used for the JLAS.

Concurrent measurements are usually obtained from the code-division scheme or the frequency-division scheme. The typical example of the code-division scheme is the global positioning system (GPS), which is susceptible to the near-far effect, leading to interference and degraded performance [30], [31]. The typical example of the frequency-division scheme is the GLONASS, which relies on complex radio frequency front-end designs, customized for various narrow frequency bands on each satellite, to mitigate interference, which incurs significant costs [32], [33]. In contrast, the TD broadcast systems are not affected by near-far effect or large bandwidth occupancy. In the TD broadcast systems, ANs periodically broadcast signals in predefined time slots, while UNs passively receive these signals and obtain sequential measurements [27]. Therefore, the TD broadcast system stands out for its ability to support an unlimited number of UNs while enhancing the safety of UNs during the localization process due to UNs' "silent" receiving-only working mode. As a result, the TD broadcast system has garnered increased attention, leading to extensive research efforts in the field of JLAS techniques in this system in recent years [12], [13], [27], [28], [29], [34], [35], [36], [37], [38].

For the JLAS taking advantage of the sequential one-way TOA and Doppler shift measurements in the TD broadcast systems, only one iterative method [39] has been proposed in the existing literature. In [39], the proposed iterative approach achieves higher estimation accuracy compared with the conventional TOA-only iterative method. However, this method is prone to nonconvergence or convergence to a local optimum without a precise initial guess, thereby causing poor robustness.

In this article, we focus on the TD broadcast systems for the JLAS, which differ from the concurrent measurement systems. The main contributions of this article are summarized as follows.

1) Taking advantage of the sequential one-way TOA and Doppler shift measurements, we formulate an objective function to solve the JLAS problem in the TD broadcast system with the AN position error, which is high-dimensional nonlinear and nonconvex. We propose a novel SDR method to relax this complex and nonconvex JLAS problem into a convex and tractable semidefinite programming (SDP) problem. Unlike the existing iterative method [39], which usually suffers from the local minima or nonconvergence without an accurate initial guess, the novel SDP method can guarantee the global optimal solution without requiring an initial guess under small Gaussian noise.
2) We conduct a theoretical error analysis, which proves that the proposed constrained WLS (CWLS) solution attains CRLB accuracy under small Gaussian noise. We evaluate the performance of the novel SDP method using 5000 Monte-Carlo simulations. Numerical results show that the proposed SDP method reaches the CRLB under small Gaussian noise. Compared with the iterative approach [39], the novel SDP method is more robust and obtains the global optimal solution without initialization under small Gaussian noise.

The rest of this article is organized as follows. In Section II, we present the system model and formulate the one-way TOA and Doppler shift measurements models. We develop a new SDP method in Section III. The CRLB and the theoretical error analysis are provided in Section IV. Section V presents the simulation results, followed by the conclusion in Section VI.

Main notations are listed in Nomenclature.

II. Problem Formulation

A. TD Broadcast LAS System Model

In a TD broadcast LAS (TDBLAS) system, there are M ANs located at known positions and a set of moving UNs with unknown positions, clock offsets, and clock drifts. We denote the inaccurate K-dimensional ($K = 2$ or 3) coordinate of the ith AN by $\boldsymbol{q}_i$, which is modeled as

$$\boldsymbol{q}_i = \boldsymbol{q}_i^o + \boldsymbol{\varepsilon}_{\boldsymbol{q}_i}, \quad i = 1, \ldots, M \tag{1}$$

where $\boldsymbol{q}_i^o$ is the true but unknown coordinate of the ith AN and $\boldsymbol{\varepsilon}_{\boldsymbol{q}_i}$ is a zero-mean Gaussian vector with a covariance matrix $\sigma_{\boldsymbol{q}_i}^2 \boldsymbol{I}_K$ [40], [41], [42], [43]. All ANs are synchronized with a centralized system clock and broadcast wireless signals periodically in a TD manner. UNs sequentially capture the signals and extract the one-way TOA and Doppler shift measurements within uniform intervals denoted by Δt, as illustrated in Fig. 1.

We represent the unknown position, velocity, clock offset, and clock drift of UNs at the beginning of one broadcast round as $\boldsymbol{p}$, $\boldsymbol{v}$, ζ, and ω, respectively. UNs' position and velocity also exist in K-dimensions. Furthermore, a TD broadcast round involving all ANs is notably brief, typically operating at the millisecond level. Consequently, we assume that the velocity and clock drift of the moving UNs remain constant through the short interval. We aim to solve the JLAS problem for the moving UNs with clock offset and clock drift based on the sequential one-way TOA and Doppler shift measurements in one broadcast round. Detailed modeling of the one-way TOA and Doppler shift measurements is presented in Section II-B.

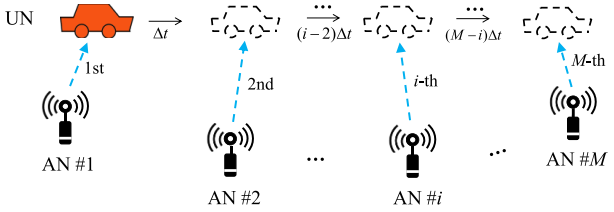

Fig. 1. TDBLAS system is composed of ANs and UNs. ANs with position errors broadcast the signals sequentially. UNs receive the signals from ANs and extract the one-way TOA and Doppler shift measurements. The position and clock offset of the moving UNs vary over time.

B. One-Way TOA and Doppler Shift Measurement Model

The sequential one-way TOA measurement arises from the difference between UNs' reception timestamp and the AN #i's transmission timestamp, which is denoted by ρ_i. We model it as

$$\begin{aligned}\rho_i &= \|\boldsymbol{q}_i^o - \boldsymbol{p} - \boldsymbol{v}\Delta t_i\| + \zeta + \omega\Delta t_i + \varepsilon_{\rho_i} \\ &= \rho_i^o + \varepsilon_{\rho_i}, \quad i = 1, \ldots, M\end{aligned} \tag{2}$$

where Δt_i represents the time interval between the initial time of the TD broadcast round and the reception time of the broadcast signal from the AN #i, that is, $\Delta t_i = \Delta t(i-1)$, ρ_i^o is the true distance, and ε_{ρ_i} is the measurement noise, following an independent zero-mean Gaussian distribution with the variance of $\sigma_{\rho_i}^2$, that is, $\varepsilon_{\rho_i} \sim \mathcal{N}(0, \sigma_{\rho_i}^2)$, and all the time-related terms ρ_i, ζ, and $\omega\Delta t_i$ are scaled by the signal propagation speed, resulting in their unit being expressed in meters.

We assume that the frequency between ANs and UNs is synchronized. By dividing the Doppler shift by the frequency of the local oscillator and then multiplying by the propagation speed of the signals, we can obtain the Doppler shift measurement, denoted by d_i, as written by

$$\begin{aligned}d_i &= -\boldsymbol{v}^T \frac{\boldsymbol{q}_i^o - \boldsymbol{p} - \boldsymbol{v}\Delta t_i}{\|\boldsymbol{q}_i^o - \boldsymbol{p} - \boldsymbol{v}\Delta t_i\|} + \omega + \varepsilon_{d_i} \\ &= d_i^o + \varepsilon_{d_i}, \quad i = 1, \ldots, M\end{aligned} \tag{3}$$

where d_i^o is the true value and ε_{d_i} is the measurement noise following an independent zero-mean Gaussian distribution with a variance of $\sigma_{d_i}^2$, that is, $\varepsilon_{d_i} \sim \mathcal{N}(0, \sigma_{d_i}^2)$.

The JLAS problem of the moving UNs in the TDB system is to estimate UNs' parameters $\boldsymbol{p}$, $\boldsymbol{v}$, ζ, and ω. We introduce a novel SDP approach to resolve the above problem. Details of the method are given in Section III.

III. New SDP Method for JLAS

In this section, we develop a new SDP method to solve the JLAS problem. First, using the maximum likelihood (ML) method, we formulate an objective function that is high-dimensional nonlinear and nonconvex. Subsequently, we define the optimization variable and formulate a nonlinear and nonconvex CWLS problem. In the final step, we propose a novel SDR approach, effectively relaxing the complex and nonconvex CWLS problem into a convex and tractable SDP problem and yielding the ultimate global optimum. The steps are as follows.

A. ML Estimator

The vector of the unknown parameter is

$$\boldsymbol{\theta} = \left[\boldsymbol{p}^T, \boldsymbol{v}^T, \zeta, \omega\right]^T. \tag{4}$$

The relationship between the stacked measurements, denoted by $\boldsymbol{\gamma}$, and the unknown parameters can be described by

$$\boldsymbol{\gamma} = \left[\boldsymbol{\rho}^T, \boldsymbol{d}^T\right]^T = h(\boldsymbol{\theta}) + \boldsymbol{\varepsilon} \tag{5}$$

where $\boldsymbol{\rho}$ and $\boldsymbol{d}$ are the collective forms of the one-way TOA measurements and Doppler shift measurements, respectively, that is, $\boldsymbol{\rho} = [\rho_1, \ldots, \rho_M]^T$ and $\boldsymbol{d} = [d_1, \ldots, d_M]^T$, $\boldsymbol{\varepsilon}$ collectively represents all the measurement noises, that is, $\boldsymbol{\varepsilon} = [\boldsymbol{\varepsilon_\rho}^T, \boldsymbol{\varepsilon_d}^T]^T = [\varepsilon_{\rho_1}, \ldots, \varepsilon_{\rho_M}, \varepsilon_{d_1}, \ldots, \varepsilon_{d_M}]^T$, $\boldsymbol{\varepsilon_\rho}$ and $\boldsymbol{\varepsilon_d}$ are modeled as the zero-mean Gaussian distributions with covariance matrices $\boldsymbol{\Sigma}_{\boldsymbol{\rho}}$ and $\boldsymbol{\Sigma}_{\boldsymbol{d}}$, respectively,

$$\begin{aligned} \boldsymbol{\Sigma}_{\boldsymbol{\rho}} &= \operatorname{diag}\left(\sigma_{\rho_1}^2, \ldots, \sigma_{\rho_M}^2\right) \\ \boldsymbol{\Sigma}_{\boldsymbol{d}} &= \operatorname{diag}\left(\sigma_{d_1}^2, \ldots, \sigma_{d_M}^2\right) \end{aligned} \tag{6}$$

and the function $h(\boldsymbol{\theta})$ is a high-dimensional nonlinear and nonconvex function which can be collectively represented by (2) and (3), that is,

$$[h(\boldsymbol{\theta})]_i = \begin{cases} \left\|\boldsymbol{q}_i^o - \boldsymbol{p} - \boldsymbol{v}\Delta t_i\right\| + \zeta + \omega\Delta t_i \\ \qquad\qquad i = 1, \ldots, M \\ -\boldsymbol{v}^T \dfrac{\boldsymbol{q}_{i-M}^o - \boldsymbol{p} - \boldsymbol{v}\Delta t_{i-M}}{\left\|\boldsymbol{q}_{i-M}^o - \boldsymbol{p} - \boldsymbol{v}\Delta t_{i-M}\right\|} + \omega \\ \qquad\qquad i = M+1, \ldots, 2M \end{cases} \tag{7}$$

where $[\cdot]_i$ represents the ith element of a vector.

Since all the measurement noise terms are independent and follow a Gaussian distribution, in accordance with (5), the ML estimation problem can be formulated as

$$\hat{\boldsymbol{\theta}} = \arg\min_{\boldsymbol{\theta}} (\boldsymbol{\gamma} - h(\boldsymbol{\theta}))^T \boldsymbol{W} (\boldsymbol{\gamma} - h(\boldsymbol{\theta})) \tag{8}$$

where $\hat{\boldsymbol{\theta}}$ is the estimator and $\boldsymbol{W}$ is a diagonal positive definite weighting matrix given by

$$\boldsymbol{W} = \operatorname{diag}\left(\boldsymbol{W}_\rho, \boldsymbol{W}_d\right) \tag{9}$$

with

$$\boldsymbol{W}_\rho = \operatorname{diag}\left(1/\sigma_{\rho_1}^2, \ldots, 1/\sigma_{\rho_M}^2\right) \tag{10}$$

$$\boldsymbol{W}_d = \operatorname{diag}\left(1/\sigma_{d_1}^2, \ldots, 1/\sigma_{d_M}^2\right). \tag{11}$$

B. Pseudo-Linearization

Substituting (1) into (2), the one-way TOA measurement is equivalent to

$$\begin{aligned} &\left\|\boldsymbol{q}_i - \boldsymbol{p} - \boldsymbol{v}\Delta t_i - \boldsymbol{\varepsilon}_{\boldsymbol{q}_i}\right\| \\ &\quad = \rho_i - \zeta - \omega\Delta t_i - \varepsilon_{\rho_i}, \quad i = 1, \ldots, M. \end{aligned} \tag{12}$$

Squaring both sides of (12) at the same time, we come to

$$\begin{aligned} &\left\|\boldsymbol{q}_i\right\|^2 - 2\boldsymbol{q}_i^T(\boldsymbol{p} + \boldsymbol{v}\Delta t_i) + \|\boldsymbol{p}\|^2 + 2\boldsymbol{p}^T\boldsymbol{v}\Delta t_i + \|\boldsymbol{v}\|^2\Delta t_i^2 \\ &\quad + \left\|\boldsymbol{\varepsilon}_{\boldsymbol{q}_i}\right\|^2 + 2(\boldsymbol{p}^T + \boldsymbol{v}^T\Delta t_i - \boldsymbol{q}_i^T)\boldsymbol{\varepsilon}_{\boldsymbol{q}_i} \\ &= (\rho_i - \varepsilon_{\rho_i})^2 + (\zeta + \omega\Delta t_i)^2 - 2(\rho_i - \varepsilon_{\rho_i})(\zeta + \omega\Delta t_i) \\ &\qquad\qquad i = 1, \ldots, M. \end{aligned} \tag{13}$$

Rearranging (13) and ignoring the second-order error terms, we have

$$\begin{aligned} &-2\boldsymbol{q}_i^T\boldsymbol{p} - 2\boldsymbol{q}_i^T\boldsymbol{v}\Delta t_i + 2\rho_i\zeta + 2\rho_i\Delta t_i\omega + \|\boldsymbol{p}\|^2 \\ &\quad + \|\boldsymbol{v}\|^2\Delta t_i^2 + 2\boldsymbol{p}^T\boldsymbol{v}\Delta t_i - \zeta^2 - \omega^2\Delta t_i^2 - 2\zeta\omega\Delta t_i \\ &\approx \rho_i^2 - \left\|\boldsymbol{q}_i\right\|^2 + 2\varepsilon_{\rho_i}(\zeta + \omega\Delta t_i - \rho_i) \\ &\quad + 2\boldsymbol{\varepsilon}_{\boldsymbol{q}_i}(\boldsymbol{q}_i^T - \boldsymbol{q}^T - \boldsymbol{v}^T\Delta t_i), \quad i = 1, \ldots, M. \end{aligned} \tag{14}$$

By observing (14), we, therefore, construct the optimization variable as

$$\boldsymbol{y} = \left[\boldsymbol{p}^T, \boldsymbol{v}^T, \zeta, \omega, \|\boldsymbol{p}\|^2, \|\boldsymbol{v}\|^2, \boldsymbol{p}^T\boldsymbol{v}, \zeta^2, \omega^2, \zeta\omega\right]^T. \tag{15}$$

We express the equation set (14) in matrix form as

$$\boldsymbol{A}_1\boldsymbol{y} - \boldsymbol{b}_1 = \boldsymbol{C}_1\boldsymbol{\varepsilon}_{\boldsymbol{\rho}} + \boldsymbol{L}_1\boldsymbol{\varepsilon}_{\boldsymbol{q}} \tag{16}$$

where

$$\boldsymbol{A}_1 = \begin{bmatrix} -2\boldsymbol{q}_1^T & -2\boldsymbol{q}_1^T\Delta t_1 & 2\rho_1 & 2\rho_1\Delta t_1 & 1 & \Delta t_1^2 & 2\Delta t_1 & -1 & -\Delta t_1^2 & -2\Delta t_1 \\ \vdots & \vdots & \vdots & \vdots & \vdots & \vdots & \vdots & \vdots & \vdots & \vdots \\ -2\boldsymbol{q}_M^T & -2\boldsymbol{q}_M^T\Delta t_M & 2\rho_M & 2\rho_M\Delta t_M & 1 & \Delta t_M^2 & 2\Delta t_M & -1 & -\Delta t_M^2 & -2\Delta t_M \end{bmatrix} \tag{17}$$

$$\boldsymbol{b}_1 = \begin{bmatrix} \rho_1^2 - \left\|\boldsymbol{q}_1\right\|^2 \\ \vdots \\ \rho_M^2 - \left\|\boldsymbol{q}_M\right\|^2 \end{bmatrix} \tag{18}$$

$$\boldsymbol{C}_1 = -2\operatorname{diag}\{(\rho_1 - \zeta - \omega\Delta t_1), \ldots, (\rho_M - \zeta - \omega\Delta t_M)\} \tag{19}$$

$$\boldsymbol{L}_1 = 2\operatorname{diag}\left\{\left(\boldsymbol{q}_1^T - \boldsymbol{p}^T - \boldsymbol{v}^T\Delta t_1\right), \ldots, \left(\boldsymbol{q}_M^T - \boldsymbol{p}^T - \boldsymbol{v}^T\Delta t_M\right)\right\} \tag{20}$$

$$\boldsymbol{\varepsilon}_{\boldsymbol{q}} = \left[\boldsymbol{\varepsilon}_{\boldsymbol{q}_1}^T, \ldots, \boldsymbol{\varepsilon}_{\boldsymbol{q}_M}^T\right]^T \tag{21}$$

with diag{·} denoting a diagonal matrix constructed from the elements inside.

Furthermore, substituting (12) into the Doppler shift measurement (3) generates

$$d_i = -\boldsymbol{v}^T \frac{\boldsymbol{q}_i - \boldsymbol{p} - \boldsymbol{v}\Delta t_i - \boldsymbol{\varepsilon}_{\boldsymbol{q}_i}}{\rho_i - \zeta - \omega\Delta t_i - \varepsilon_{\rho_i}} + \omega + \varepsilon_{d_i}, \quad i = 1, \ldots, M. \tag{22}$$

Multiplying both sides of (22) by $(\rho_i - \zeta - \omega\Delta t_i - \varepsilon_{\rho_i})$, sorting, and ignoring the second-order error terms, we have

$$\boldsymbol{q}_i^T\boldsymbol{v} - d_i\zeta - (d_i\Delta t_i + \rho_i)\omega - \|\boldsymbol{v}\|^2\Delta t_i - \boldsymbol{p}^T\boldsymbol{v} + \omega^2\Delta t_i + \zeta\omega$$

$$\approx -d_i\rho_i + \varepsilon_{\rho_i}(d_i-\omega) + \varepsilon_{d_i}(\rho_i-\zeta-\omega\Delta t_i) + \boldsymbol{v}^T\boldsymbol{\varepsilon}_{\boldsymbol{q}_i} \quad i=1,\ldots,M. \tag{23}$$

Similarly, (23) can be expressed as

$$\boldsymbol{A}_2\boldsymbol{y}-\boldsymbol{b}_2 = \boldsymbol{C}_2\boldsymbol{\varepsilon}_{\boldsymbol{\rho}} + \boldsymbol{D}_2\boldsymbol{\varepsilon}_{\boldsymbol{d}} + \boldsymbol{L}_2\boldsymbol{\varepsilon}_{\boldsymbol{q}} \tag{24}$$

where

$$\boldsymbol{A}_2 = \begin{bmatrix} \boldsymbol{0}_{1\times K} & \boldsymbol{q}_1^T & -d_1 & -(d_1\Delta t_1+\rho_1) & 0 & -\Delta t_1 & -1 & 0 & \Delta t_1 & 1 \\ \vdots & \vdots & \vdots & \vdots & \vdots & \vdots & \vdots & \vdots & \vdots & \vdots \\ \boldsymbol{0}_{1\times K} & \boldsymbol{q}_M^T & -d_M & -(d_M\Delta t_M+\rho_M) & 0 & -\Delta t_M & -1 & 0 & \Delta t_M & 1 \end{bmatrix} \tag{25}$$

$$\boldsymbol{b}_2 = \begin{bmatrix} -d_1\rho_1 \\ \vdots \\ -d_M\rho_M \end{bmatrix} \tag{26}$$

$$\boldsymbol{C}_2 = \mathrm{diag}\{(d_1-\omega),\ldots,(d_M-\omega)\} \tag{27}$$

$$\boldsymbol{D}_2 = \mathrm{diag}\{(\rho_1-\zeta-\omega\Delta t_1),\ldots,(\rho_M-\zeta-\omega\Delta t_M)\} \tag{28}$$

$$\boldsymbol{L}_2 = \mathrm{diag}\big\{(\boldsymbol{v}^T),\ldots,(\boldsymbol{v}^T)\big\}_{M\times MK}. \tag{29}$$

Therefore, we combine (16) and (24) and come to

$$\boldsymbol{A}\boldsymbol{y}-\boldsymbol{b} = \boldsymbol{C}\boldsymbol{\varepsilon}_{\boldsymbol{\rho}} + \boldsymbol{D}\boldsymbol{\varepsilon}_{\boldsymbol{d}} + \boldsymbol{L}\boldsymbol{\varepsilon}_{\boldsymbol{q}} \tag{30}$$

where

$$\boldsymbol{A} = \begin{bmatrix} \boldsymbol{A}_1 \\ \boldsymbol{A}_2 \end{bmatrix}_{2M\times(2K+8)}, \quad \boldsymbol{b} = \begin{bmatrix} \boldsymbol{b}_1 \\ \boldsymbol{b}_2 \end{bmatrix}_{2M\times 1}$$
$$\boldsymbol{C} = \begin{bmatrix} \boldsymbol{C}_1 \\ \boldsymbol{C}_2 \end{bmatrix}_{2M\times M}, \quad \boldsymbol{D} = \begin{bmatrix} \boldsymbol{0} \\ \boldsymbol{D}_2 \end{bmatrix}_{2M\times M} \tag{31}$$

$$\boldsymbol{L} = \begin{bmatrix} \boldsymbol{L}_1 \\ \boldsymbol{L}_2 \end{bmatrix}_{2M\times MK}. \tag{32}$$

According to (30), we formulate the following CWLS problem:

$$\boldsymbol{J}(\boldsymbol{y}) \triangleq \arg\min_{\boldsymbol{y}} (\boldsymbol{A}\boldsymbol{y}-\boldsymbol{b})^T\boldsymbol{R}^{-1}(\boldsymbol{A}\boldsymbol{y}-\boldsymbol{b}) \tag{33}$$

where

$$\boldsymbol{R} = \boldsymbol{C}\boldsymbol{W}_{\rho}^{-1}\boldsymbol{C}^T + \boldsymbol{D}\boldsymbol{W}_{d}^{-1}\boldsymbol{D}^T + \boldsymbol{L}\boldsymbol{W}_{\boldsymbol{q}}^{-1}\boldsymbol{L}^T \tag{34}$$

with $\boldsymbol{W}_{\boldsymbol{q}}^{-1} = \mathrm{diag}\{(1/\sigma_{\boldsymbol{q}_1})\boldsymbol{I}_K,\ldots,(1/\sigma_{\boldsymbol{q}_M})\boldsymbol{I}_K\}$.

Applying the implicit relationship between the elements of $\boldsymbol{y}$, the CWLS problem in (33) is equivalently expressed as

$$\min_{\boldsymbol{y}} (\boldsymbol{A}\boldsymbol{y}-\boldsymbol{b})^T\boldsymbol{R}^{-1}(\boldsymbol{A}\boldsymbol{y}-\boldsymbol{b}) \tag{35a}$$
$$\text{s.t. } \|[\boldsymbol{y}]_{1:K}\|^2 = [\boldsymbol{y}]_{2K+3} \tag{35b}$$
$$\|[\boldsymbol{y}]_{K+1:2K}\|^2 = [\boldsymbol{y}]_{2K+4} \tag{35c}$$
$$[\boldsymbol{y}]_{1:K}^T[\boldsymbol{y}]_{K+1:2K} = [\boldsymbol{y}]_{2K+5} \tag{35d}$$
$$[\boldsymbol{y}]_{2K+1}^2 = [\boldsymbol{y}]_{2K+6} \tag{35e}$$
$$[\boldsymbol{y}]_{2K+2}^2 = [\boldsymbol{y}]_{2K+7} \tag{35f}$$
$$[\boldsymbol{y}]_{2K+1}[\boldsymbol{y}]_{2K+2} = [\boldsymbol{y}]_{2K+8} \tag{35g}$$
$$[\boldsymbol{y}]_{2K+1}[\boldsymbol{y}]_{2K+8} = [\boldsymbol{y}]_{2K+2}[\boldsymbol{y}]_{2K+6} \tag{35h}$$
$$[\boldsymbol{y}]_{2K+2}[\boldsymbol{y}]_{2K+8} = [\boldsymbol{y}]_{2K+1}[\boldsymbol{y}]_{2K+7}. \tag{35i}$$

C. SDP Method

The minimization problem given by (35) is high-dimensional nonlinear and nonconvex, and it involves a large number of variables, making it still difficult to find the global optimum. We propose a novel SDR method to address this challenge by transforming the problem into a convex form.

Introducing the variable $\boldsymbol{Y} = \boldsymbol{y}\boldsymbol{y}^T$ and applying the basic properties of $\boldsymbol{x}^T\boldsymbol{A}\boldsymbol{x} = \mathrm{tr}(\boldsymbol{x}\boldsymbol{x}^T\boldsymbol{A})$, the CWLS problem (35) becomes

$$\min_{\boldsymbol{Y},\boldsymbol{y}} \mathrm{tr}\left(\boldsymbol{F}\begin{bmatrix} \boldsymbol{Y} & \boldsymbol{y} \\ \boldsymbol{y}^T & 1 \end{bmatrix}\right) \tag{36a}$$
$$\text{s.t. } \boldsymbol{Y} = \boldsymbol{y}\boldsymbol{y}^T$$
$$\text{(35b)-(35i)} \tag{36b}$$

where

$$\boldsymbol{F} = \begin{bmatrix} \boldsymbol{A}^T\boldsymbol{R}^{-1}\boldsymbol{A} & -\boldsymbol{A}^T\boldsymbol{R}^{-1}\boldsymbol{b} \\ -\boldsymbol{b}^T\boldsymbol{R}^{-1}\boldsymbol{A} & \boldsymbol{b}^T\boldsymbol{R}^{-1}\boldsymbol{b} \end{bmatrix}. \tag{37}$$

By leveraging the relationship between $\boldsymbol{Y}$ and $\boldsymbol{y}$, the constraints in (35b)–(35i) can be expressed as

$$\mathrm{tr}([\boldsymbol{Y}]_{1:K,1:K}) = [\boldsymbol{y}]_{2K+3}, \tag{38a}$$
$$\mathrm{tr}([\boldsymbol{Y}]_{K+1:2K,K+1:2K}) = [\boldsymbol{y}]_{2K+4} \tag{38b}$$
$$\mathrm{tr}([\boldsymbol{Y}]_{1:K,K+1:2K}) = [\boldsymbol{y}]_{2K+5} \tag{38c}$$
$$[\boldsymbol{Y}]_{2K+1,2K+1} = [\boldsymbol{y}]_{2K+6} \tag{38d}$$
$$[\boldsymbol{Y}]_{2K+2,2K+2} = [\boldsymbol{y}]_{2K+7} \tag{38e}$$
$$[\boldsymbol{Y}]_{2K+1,2K+2} = [\boldsymbol{y}]_{2K+8} \tag{38f}$$
$$[\boldsymbol{Y}]_{2K+1,2K+8} = [\boldsymbol{Y}]_{2K+2,2K+6} \tag{38g}$$
$$[\boldsymbol{Y}]_{2K+2,2K+8} = [\boldsymbol{Y}]_{2K+1,2K+7}. \tag{38h}$$

We observe that the constraints from (38a)–(38h) exhibit linearity with respect to the variables and, therefore, they are convex. However, the constraint (36b) is still nonlinear and nonconvex.

The nonconvex constraint (36b) is equivalent as

$$\boldsymbol{Y} = \boldsymbol{y}\boldsymbol{y}^T \Leftrightarrow \begin{bmatrix} \boldsymbol{Y} & \boldsymbol{y} \\ \boldsymbol{y}^T & 1 \end{bmatrix} \succeq 0, \quad \mathrm{rank}(\boldsymbol{Y}) = 1. \tag{39}$$

By omitting the rank-1 constraint in (39), we obtain the following standard SDP problem:

$$\min_{\boldsymbol{Y},\boldsymbol{y}} \mathrm{tr}\left(\boldsymbol{F}\begin{bmatrix} \boldsymbol{Y} & \boldsymbol{y} \\ \boldsymbol{y}^T & 1 \end{bmatrix}\right) \tag{40a}$$
$$\text{s.t. } \begin{bmatrix} \boldsymbol{Y} & \boldsymbol{y} \\ \boldsymbol{y}^T & 1 \end{bmatrix} \succeq 0$$
$$\text{(38a)-(38h)}. \tag{40b}$$

We can solve the above SDP problem through off-the-shelf software. Define $\{\hat{\boldsymbol{Y}}, \hat{\boldsymbol{y}}\}$ as the solution of the SDP problem. Based on the definition of $\boldsymbol{y}$, we obtain the estimates of $\hat{\boldsymbol{p}}$, $\hat{\boldsymbol{v}}$, $\hat{\zeta}$, and $\hat{\omega}$ by

$$\hat{\boldsymbol{p}} = [\hat{\boldsymbol{y}}]_{1:K} \tag{41a}$$
$$\hat{\boldsymbol{v}} = [\hat{\boldsymbol{y}}]_{K+1,2K} \tag{41b}$$
$$\hat{\zeta} = [\hat{\boldsymbol{y}}]_{2K+1} \tag{41c}$$
$$\hat{\omega} = [\hat{\boldsymbol{y}}]_{2K+2}. \tag{41d}$$

The procedure of the new SDP method is summarized in Algorithm 1.

Algorithm 1 SDP Method

1: Input: TOA measurements $\boldsymbol{\rho}$ and Doppler shift measurements $\boldsymbol{d}$, noise covariance $\sigma_{\rho_i}^2$, $\sigma_{d_i}^2$, $\sigma_{\boldsymbol{q}_i}^2$, and the ANs' positions $\boldsymbol{q}_i$, $i = 1, \ldots, M$.
2: Step1: Set $\boldsymbol{R}^{-1}$ as identity matrix $\boldsymbol{I}_{2M\times 2M}$. Solve the SDP problem (40) and get the initial estimates for $\hat{\boldsymbol{p}}_0$, $\hat{\boldsymbol{v}}_0$, $\hat{\zeta}_0$ and $\hat{\omega}_0$.
3: Step2: Use $\hat{\boldsymbol{p}}_0$, $\hat{\boldsymbol{v}}_0$, $\hat{\zeta}_0$ and $\hat{\omega}_0$ to reconstruct the $\boldsymbol{R}^{-1}$.
4: Step3: Solve the SDP problem (40) again and get the ultimate estimation $\hat{\boldsymbol{y}}$.
5: Output: $\hat{\boldsymbol{p}}$, $\hat{\boldsymbol{v}}$, $\hat{\zeta}$, and $\hat{\omega}$.

IV. Performance Analysis

In this section, we derive the CRLB as a benchmark to represent the minimum attainable accuracy of an unbiased estimator. Subsequently, we conduct a theoretical error analysis to assess the accuracy of the CWLS solution. Additionally, we conduct the computational complexity analysis.

A. CRLB Derivation

Let $\boldsymbol{\eta} = [\boldsymbol{\theta}^T, \boldsymbol{q}^{oT}]^T$, the logarithm of the likelihood function for the unknown parameter $\boldsymbol{\theta}$ and the true AN position is

$$\ln f(\boldsymbol{\gamma}, \boldsymbol{q} \mid \boldsymbol{\eta}) = k - \frac{1}{2}(\boldsymbol{\gamma} - \boldsymbol{\gamma}^o)^T \boldsymbol{W}(\boldsymbol{\gamma} - \boldsymbol{\gamma}^o) - \frac{1}{2}(\boldsymbol{q} - \boldsymbol{q}^o)^T \boldsymbol{W}_q (\boldsymbol{q} - \boldsymbol{q}^o) \tag{42}$$

where

$$\boldsymbol{q}^o = \left[\boldsymbol{q}_1^{oT}, \ldots, \boldsymbol{q}_M^{oT}\right]^T. \tag{43}$$

The CRLB for estimating $\boldsymbol{\eta}$ is [44]

$$\begin{aligned} \mathrm{CRLB}(\boldsymbol{\eta}) &= -\left(\mathbb{E}\left[\frac{\partial^2 \ln f(\boldsymbol{\gamma}, \boldsymbol{q} \mid \boldsymbol{\eta})}{\partial \boldsymbol{\eta} \partial \boldsymbol{\eta}^T}\right]\right)^{-1} \\ &= \begin{bmatrix} \boldsymbol{X}_{11} & \boldsymbol{X}_{12} \\ \boldsymbol{X}_{12}^T & \boldsymbol{X}_{22} \end{bmatrix}^{-1} \end{aligned} \tag{44}$$

where

$$\begin{aligned} \boldsymbol{X}_{11} &= -\mathbb{E}\left[\frac{\partial^2 \ln f(\boldsymbol{\gamma}, \boldsymbol{q} \mid \boldsymbol{\eta})}{\partial \boldsymbol{\theta} \partial \boldsymbol{\theta}^T}\right] = (\nabla_{\boldsymbol{\theta}} \boldsymbol{\gamma}^o)^T \boldsymbol{W} (\nabla_{\boldsymbol{\theta}} \boldsymbol{\gamma}^o) \\ \boldsymbol{X}_{12} &= -\mathbb{E}\left[\frac{\partial^2 \ln f(\boldsymbol{\gamma}, \boldsymbol{q} \mid \boldsymbol{\eta})}{\partial \boldsymbol{\theta} \partial \boldsymbol{q}^{oT}}\right] = (\nabla_{\boldsymbol{\theta}} \boldsymbol{\gamma}^o)^T \boldsymbol{W} (\nabla_{\boldsymbol{q}^o} \boldsymbol{\gamma}^o) \\ \boldsymbol{X}_{22} &= -\mathbb{E}\left[\frac{\partial^2 \ln f(\boldsymbol{\gamma}, \boldsymbol{q} \mid \boldsymbol{\eta})}{\partial \boldsymbol{q}^o \partial \boldsymbol{q}^{oT}}\right] = (\nabla_{\boldsymbol{q}^o} \boldsymbol{\gamma}^o)^T \boldsymbol{W} (\nabla_{\boldsymbol{q}^o} \boldsymbol{\gamma}^o) + \boldsymbol{W}_q \end{aligned} \tag{45}$$

where the operator $\nabla_{\boldsymbol{a}} \boldsymbol{f}$ is the row vector partial derivative of function $\boldsymbol{f}(\boldsymbol{a})$ defined as

$$\nabla_{\boldsymbol{a}} \boldsymbol{f} = \frac{\partial \boldsymbol{f}}{\partial \boldsymbol{a}^T} \tag{46}$$

and

$$[\nabla_{\boldsymbol{\theta}} \boldsymbol{\gamma}^o]_{i,:} = \begin{cases} [-\boldsymbol{e}_i^T, -\boldsymbol{e}_i^T \Delta t_i, 1, \Delta t_i], & i = 1, \ldots, M \\ [[\nabla_{\boldsymbol{p}} \boldsymbol{d}^o]_{i-M}, [\nabla_{\boldsymbol{v}} \boldsymbol{d}^o]_{i-M}, 0, 1], & i = M+1, \ldots, 2M \end{cases} \tag{47}$$

$$\nabla_{\boldsymbol{q}^o} \boldsymbol{\gamma}^o = \begin{bmatrix} \mathrm{diag}(\nabla_{\boldsymbol{q}_1^o} \rho_1^o, \ldots, \nabla_{\boldsymbol{q}_M^o} \rho_M^o) \\ \mathrm{diag}(\nabla_{\boldsymbol{q}_1^o} d_1^o, \ldots, \nabla_{\boldsymbol{q}_M^o} d_M^o) \end{bmatrix} \tag{48}$$

$$\boldsymbol{\rho}^o = \left[\rho_1^o, \ldots, \rho_M^o\right]^T \tag{49}$$

$$\boldsymbol{d}^o = \left[d_1^o, \ldots, d_M^o\right]^T \tag{50}$$

$$\boldsymbol{e}_i = \frac{\boldsymbol{q}_i^o - \boldsymbol{p} - \boldsymbol{v}\Delta t_i}{\|\boldsymbol{q}_i^o - \boldsymbol{p} - \boldsymbol{v}\Delta t_i\|}, \quad i = 1, \ldots, M \tag{51}$$

$$\begin{aligned} [\nabla_{\boldsymbol{p}} \boldsymbol{d}^o]_{i-M} &= \frac{\boldsymbol{v}^T}{\|\boldsymbol{q}_{i-M}^o - \boldsymbol{p} - \boldsymbol{v}\Delta t_{i-M}\|} \\ &\quad - \frac{\boldsymbol{v}^T (\boldsymbol{q}_{i-M}^o - \boldsymbol{p} - \boldsymbol{v}\Delta t_{i-M})(\boldsymbol{q}_{i-M}^o - \boldsymbol{p} - \boldsymbol{v}\Delta t_{i-M})^T}{\|\boldsymbol{q}_{i-M}^o - \boldsymbol{p} - \boldsymbol{v}\Delta t_{i-M}\|^3} \\ &\quad i = M+1, \ldots, 2M \end{aligned} \tag{52}$$

$$\begin{aligned} [\nabla_{\boldsymbol{v}} \boldsymbol{d}^o]_{i-M} &= \frac{2\boldsymbol{v}^T \Delta t_{i-M} + \boldsymbol{p}^T - \boldsymbol{q}_{i-M}^{oT}}{\|\boldsymbol{q}_{i-M}^o - \boldsymbol{p} - \boldsymbol{v}\Delta t_{i-M}\|} \\ &\quad - \frac{\boldsymbol{v}^T \Delta t_{i-M} (\boldsymbol{q}_{i-M}^o - \boldsymbol{p} - \boldsymbol{v}\Delta t_{i-M})(\boldsymbol{q}_{i-M}^o - \boldsymbol{p} - \boldsymbol{v}\Delta t_{i-M})^T}{\|\boldsymbol{q}_{i-M}^o - \boldsymbol{p} - \boldsymbol{v}\Delta t_{i-M}\|^3} \\ &\quad i = M+1, \ldots, 2M \end{aligned} \tag{53}$$

$$\nabla_{\boldsymbol{q}_i^o} \rho_i^o = \boldsymbol{e}_i^T, \quad i = 1, \ldots, M \tag{54}$$

$$\begin{aligned} \nabla_{\boldsymbol{q}_i^o} d_i^o &= -\frac{\boldsymbol{v}^T}{\|\boldsymbol{q}_i^o - \boldsymbol{p} - \boldsymbol{v}\Delta t_i\|} \\ &\quad + \frac{\boldsymbol{v}^T (\boldsymbol{q}_i^o - \boldsymbol{p} - \boldsymbol{v}\Delta t_i)(\boldsymbol{q}_i^o - \boldsymbol{p} - \boldsymbol{v}\Delta t_i)^T}{\|\boldsymbol{q}_i^o - \boldsymbol{p} - \boldsymbol{v}\Delta t_i\|^3} \\ &\quad i = 1, \ldots, M. \end{aligned} \tag{55}$$

The CRLB for estimating $\boldsymbol{\theta}$ is [29]

$$\mathrm{CRLB}(\boldsymbol{\theta}) = \left(\boldsymbol{X}_{11} - \boldsymbol{X}_{12} \boldsymbol{X}_{22}^{-1} \boldsymbol{X}_{12}^T\right)^{-1}. \tag{56}$$

B. Theoretical Errors Analysis

We now first analyze the theoretical errors of the CWLS solution. Then, we prove that the CWLS solution reaches the CRLB under the low Gaussian noise condition.

Denote the estimation results of the CWLS problem (35) as

$$\hat{\boldsymbol{\theta}} = \left[\hat{\boldsymbol{p}}^T, \hat{\boldsymbol{v}}^T, \hat{\zeta}, \hat{\omega}\right]^T. \tag{57}$$

According to (33), $\hat{\boldsymbol{\theta}}$ satisfies

$$\boldsymbol{g}(\hat{\boldsymbol{\theta}}) = \left.\frac{\partial \boldsymbol{J}}{\partial \boldsymbol{\theta}}\right|_{\boldsymbol{\theta}=\hat{\boldsymbol{\theta}}} = 0. \tag{58}$$

At the low-noise levels, where the estimated parameter $\hat{\boldsymbol{\theta}}$ is close to the true value $\boldsymbol{\theta}^o$, we apply the Taylor series expansion to (58), omitting terms of second order and beyond. This yields

$$\left.\frac{\partial \boldsymbol{J}}{\partial \boldsymbol{\theta}}\right|_{\boldsymbol{\theta}=\hat{\boldsymbol{\theta}}} \approx \left.\frac{\partial \boldsymbol{J}}{\partial \boldsymbol{\theta}}\right|_{\boldsymbol{\theta}=\boldsymbol{\theta}^o} + \left.\frac{\partial^2 \boldsymbol{J}}{\partial \boldsymbol{\theta}\partial \boldsymbol{\theta}^T}\right|_{\boldsymbol{\theta}=\boldsymbol{\theta}^o} (\hat{\boldsymbol{\theta}} - \boldsymbol{\theta}^o) \approx 0 \tag{59}$$

that is,

$$\boldsymbol{g}(\hat{\boldsymbol{\theta}}) \approx \boldsymbol{g}(\boldsymbol{\theta}^o) + \boldsymbol{H}(\boldsymbol{\theta}^o)(\hat{\boldsymbol{\theta}} - \boldsymbol{\theta}^o) \approx 0 \tag{60}$$

where $\boldsymbol{g}(\boldsymbol{\theta}^o)$ and $\boldsymbol{H}(\boldsymbol{\theta}^o)$ are the corresponding gradient vector and Hessian matrix evaluated at the true location, respectively, expressed as

$$\boldsymbol{g}(\boldsymbol{\theta}^o) = \left.\frac{\partial \boldsymbol{J}}{\partial \boldsymbol{\theta}}\right|_{\boldsymbol{\theta}=\boldsymbol{\theta}^o}, \quad \boldsymbol{H}(\boldsymbol{\theta}^o) = \left.\frac{\partial^2 \boldsymbol{J}}{\partial \boldsymbol{\theta}\partial \boldsymbol{\theta}^T}\right|_{\boldsymbol{\theta}=\boldsymbol{\theta}^o}. \tag{61}$$

Following (60), the estimation error is written as

$$\Delta\boldsymbol{\theta} \triangleq \hat{\boldsymbol{\theta}} - \boldsymbol{\theta}^o \approx -\boldsymbol{H}(\boldsymbol{\theta}^o)^{-1}\boldsymbol{g}(\boldsymbol{\theta}^o). \tag{62}$$

Using (33), the gradient vector and the Hessian matrix are expressed as

$$\boldsymbol{g}(\boldsymbol{\theta}^o) = -2\boldsymbol{G}^T\boldsymbol{R}^{-1}(\boldsymbol{b} - \boldsymbol{A}\boldsymbol{y}^o) \tag{63}$$

$$\boldsymbol{H}(\boldsymbol{\theta}^o) = 2\boldsymbol{G}^T\boldsymbol{R}^{-1}\boldsymbol{G} \tag{64}$$

where

$$\boldsymbol{G} = \left[\boldsymbol{G}_p, \boldsymbol{G}_v, \boldsymbol{G}_b, \boldsymbol{G}_\omega\right] \tag{65}$$

with

$$\boldsymbol{G}_p \triangleq \left.\frac{\partial(\boldsymbol{A}\boldsymbol{y})}{\partial \boldsymbol{p}^T}\right|_{\boldsymbol{\theta}=\boldsymbol{\theta}^o} = \begin{bmatrix} -2(\boldsymbol{q}_1 - \boldsymbol{p} - \boldsymbol{v}\Delta t_1)^T \\ \vdots \\ -2(\boldsymbol{q}_M - \boldsymbol{p} - \boldsymbol{v}\Delta t_M)^T \\ -\boldsymbol{v}^T \\ \vdots \\ -\boldsymbol{v}^T \end{bmatrix}_{2M\times K} \tag{66}$$

$$\boldsymbol{G}_v \triangleq \left.\frac{\partial(\boldsymbol{A}\boldsymbol{y})}{\partial \boldsymbol{v}^T}\right|_{\boldsymbol{\theta}=\boldsymbol{\theta}^o} = \begin{bmatrix} -2\Delta t_1(\boldsymbol{q}_1 - \boldsymbol{p} - \boldsymbol{v}\Delta t_1)^T \\ \vdots \\ -2\Delta t_M(\boldsymbol{q}_M - \boldsymbol{p} - \boldsymbol{v}\Delta t_M)^T \\ (\boldsymbol{q}_1 - \boldsymbol{p} - 2\boldsymbol{v}\Delta t_1)^T \\ \vdots \\ (\boldsymbol{q}_M - \boldsymbol{p} - 2\boldsymbol{v}\Delta t_M)^T \end{bmatrix}_{2M\times K} \tag{67}$$

$$\boldsymbol{G}_b \triangleq \left.\frac{\partial(\boldsymbol{A}\boldsymbol{y})}{\partial \zeta}\right|_{\boldsymbol{\theta}=\boldsymbol{\theta}^o} = \begin{bmatrix} 2(\rho_1 - \zeta - \omega\Delta t_1) \\ \vdots \\ 2(\rho_M - \zeta - \omega\Delta t_M) \\ -(d_1 - \omega) \\ \vdots \\ -(d_M - \omega) \end{bmatrix}_{2M\times 1} \tag{68}$$

$$\boldsymbol{G}_\omega \triangleq \left.\frac{\partial(\boldsymbol{A}\boldsymbol{y})}{\partial \omega}\right|_{\boldsymbol{\theta}=\boldsymbol{\theta}^o} = \begin{bmatrix} 2\Delta t_1(\rho_1 - \zeta - \omega\Delta t_1) \\ \vdots \\ 2\Delta t_M(\rho_M - \zeta - \omega\Delta t_M) \\ -(\rho_1 - \zeta - \omega\Delta t_1) - (d_1 - \omega)\Delta t_1 \\ \vdots \\ -(\rho_M - \zeta - \omega\Delta t_M) - (d_M - \omega)\Delta t_M \end{bmatrix}_{2M\times 1}. \tag{69}$$

Substituting (63) and (64) into (62) yields

$$\Delta\boldsymbol{\theta} \approx (\boldsymbol{G}^T\boldsymbol{R}^{-1}\boldsymbol{G})^{-1}\boldsymbol{G}^T\boldsymbol{R}^{-1}(\boldsymbol{b} - \boldsymbol{A}\boldsymbol{y}^o) \tag{70}$$

where the matrix $\boldsymbol{G}$ is related to the true value $\boldsymbol{G}^o$ and the measurement noise $\Delta\boldsymbol{G}$, and it can be written as

$$\boldsymbol{G} = \boldsymbol{G}^o + \Delta\boldsymbol{G}. \tag{71}$$

Substituting (1) into (66)–(69), the expansion of $\boldsymbol{G}^o$ can be written as (72), as shown at the bottom of the next page, and

$$\Delta\boldsymbol{G} = \begin{bmatrix} -2\boldsymbol{\varepsilon}_{\boldsymbol{q}_1}^T & -2\Delta t_1\boldsymbol{\varepsilon}_{\boldsymbol{q}_1}^T & 2\varepsilon_{\rho_1} & 2\Delta t_1\varepsilon_{\rho_1} \\ \vdots & \vdots & \vdots & \vdots \\ -2\boldsymbol{\varepsilon}_{\boldsymbol{q}_M}^T & -2\Delta t_M\boldsymbol{\varepsilon}_{\boldsymbol{q}_M}^T & 2\varepsilon_{\rho_M} & 2\Delta t_M\varepsilon_{\rho_M} \\ \boldsymbol{0}_{1\times K} & \boldsymbol{\varepsilon}_{\boldsymbol{q}_1}^T & -\varepsilon_{d_1} & -\varepsilon_{\rho_1} - \varepsilon_{d_1} \\ \vdots & \vdots & \vdots & \vdots \\ \boldsymbol{0}_{1\times K} & \boldsymbol{\varepsilon}_{\boldsymbol{q}_M}^T & -\varepsilon_{d_M} & -\varepsilon_{\rho_M} - \varepsilon_{d_M} \end{bmatrix}. \tag{79}$$

Similarly, matrix $\boldsymbol{R}$ is written as

$$\begin{aligned} \boldsymbol{R} &= \boldsymbol{C}\boldsymbol{W}_\rho^{-1}\boldsymbol{C}^T + \boldsymbol{D}\boldsymbol{W}_d^{-1}\boldsymbol{D}^T + \boldsymbol{L}\boldsymbol{W}_{\boldsymbol{q}}^{-1}\boldsymbol{L}^T \\ &= \boldsymbol{R}^o + \Delta\boldsymbol{R} \end{aligned} \tag{80}$$

where

$$\begin{aligned} \boldsymbol{C} &= \boldsymbol{C}^o + \Delta\boldsymbol{C} = \begin{bmatrix} \boldsymbol{C}_1^o \\ \boldsymbol{C}_2^o \end{bmatrix} + \begin{bmatrix} \Delta\boldsymbol{C}_1 \\ \Delta\boldsymbol{C}_2 \end{bmatrix} \\ \boldsymbol{D} &= \boldsymbol{D}^o + \Delta\boldsymbol{D} = \begin{bmatrix} \boldsymbol{0} \\ \boldsymbol{D}_2^o \end{bmatrix} + \begin{bmatrix} \Delta\boldsymbol{0} \\ \Delta\boldsymbol{D}_2 \end{bmatrix} \\ \boldsymbol{L} &= \boldsymbol{L}^o + \Delta\boldsymbol{L} = \begin{bmatrix} \boldsymbol{L}_1^o \\ \boldsymbol{L}_2^o \end{bmatrix} + \begin{bmatrix} \Delta\boldsymbol{L}_1 \\ \Delta\boldsymbol{0} \end{bmatrix} \end{aligned} \tag{81}$$

with the expansion of $\boldsymbol{C}_1^o$, $\boldsymbol{C}_2^o$, $\boldsymbol{D}_2^o$, $\boldsymbol{L}_1^o$, and $\boldsymbol{L}_2^o$ showing in (73)–(77), as shown at the bottom of the next page, and

$$\begin{aligned} \Delta\boldsymbol{C}_1 &= \mathrm{diag}\{-2\varepsilon_{\rho_1}, \ldots, -2\varepsilon_{\rho_M}\} \\ \Delta\boldsymbol{C}_2 &= \mathrm{diag}\{\varepsilon_{d_1}, \ldots, \varepsilon_{d_M}\} \\ \Delta\boldsymbol{D}_2 &= \mathrm{diag}\{\varepsilon_{\rho_1}, \ldots, \varepsilon_{\rho_M}\} \\ \Delta\boldsymbol{L}_1 &= \mathrm{diag}\left\{2\boldsymbol{\varepsilon}_{\boldsymbol{q}_1}^T, \ldots, 2\boldsymbol{\varepsilon}_{\boldsymbol{q}_M}^T\right\}. \end{aligned} \tag{82}$$

Substituting matrix $\boldsymbol{C}$, $\boldsymbol{D}$, and $\boldsymbol{L}$ in (81) into (80) yields

$$\begin{aligned} \boldsymbol{R}^o &= \begin{bmatrix} \boldsymbol{C}^o & \boldsymbol{D}^o \end{bmatrix}\boldsymbol{W}^{-1}\begin{bmatrix} \boldsymbol{C}^o & \boldsymbol{D}^o \end{bmatrix}^T + \boldsymbol{L}^o\boldsymbol{W}_{\boldsymbol{q}}{}^{-1}\boldsymbol{L}^{oT} \\ &= \boldsymbol{P}^o\boldsymbol{W}^{-1}\boldsymbol{P}^{oT} + \boldsymbol{L}^o\boldsymbol{W}_{\boldsymbol{q}}{}^{-1}\boldsymbol{L}^{oT}. \end{aligned} \tag{83}$$

By substituting (71) and (80) into (70) and keeping the terms of first order only, we obtain

$$\Delta\boldsymbol{\theta} \approx -(\boldsymbol{G}^{oT}\boldsymbol{R}^{o-1}\boldsymbol{G}^o)^{-1}\boldsymbol{G}^{oT}\boldsymbol{R}^{o-1}(\boldsymbol{C}^o\boldsymbol{\varepsilon}_\rho + \boldsymbol{D}^o\boldsymbol{\varepsilon}_d + \boldsymbol{L}^o\boldsymbol{\varepsilon}_{\boldsymbol{q}}). \tag{84}$$

Then, the covariance of the estimation error for the CWLS solution is computed as

$$\begin{aligned}\mathbb{E}\left[\Delta\boldsymbol{\theta}\Delta\boldsymbol{\theta}^T\right] &= (\boldsymbol{G}^{oT}\boldsymbol{R}^{o-1}\boldsymbol{G}^o)^{-1} \\ &= \left[\boldsymbol{G}_2^T\boldsymbol{W}\boldsymbol{G}_2 - \left(\boldsymbol{G}_2^T\boldsymbol{W}\boldsymbol{G}_1\right)\right. \\ &\quad \left.\cdot\left(\boldsymbol{G}_1^T\boldsymbol{W}\boldsymbol{G}_1 + \boldsymbol{W}_{\boldsymbol{q}}^{-1}\left(\boldsymbol{G}_2^T\boldsymbol{W}\boldsymbol{G}_1\right)^T\right]^{-1}\right. \end{aligned} \tag{85}$$

where

$$\boldsymbol{G}_1 = \boldsymbol{P}^{o-1}\boldsymbol{L}^o, \quad \boldsymbol{G}_2 = \boldsymbol{P}^{o-1}\boldsymbol{G}^o \tag{86}$$

and

$$\boldsymbol{P}^{o-1} = \begin{bmatrix}\boldsymbol{C}_1^o & \boldsymbol{0} \\ \boldsymbol{C}_2^o & \boldsymbol{D}_2^o\end{bmatrix}^{-1} = \begin{bmatrix}\boldsymbol{C}_1^{o-1} & \boldsymbol{0} \\ -\boldsymbol{D}_2^{o-1}\boldsymbol{C}_2^o\boldsymbol{C}_1^{o-1} & \boldsymbol{D}_2^{o-1}\end{bmatrix}. \tag{87}$$

Substituting (73)–(77) into (87), we can obtain the specific expansion of $\boldsymbol{P}^{o-1}$ in (78), as shown at the bottom of the page.

Comparing (85) and (56), we can derive that

$$\mathbb{E}\left[\Delta\boldsymbol{\theta}\Delta\boldsymbol{\theta}^T\right] \approx \mathrm{CRLB}(\boldsymbol{\theta}) \tag{88}$$

when the measurement errors and AN position errors are small. To conclude, the estimation error covariance of the CWLS solution reaches the CRLB under the small Gaussian noise.

In addition, according to (85) and (88), we can express the theoretical root mean square error (RMSE) of the CWLS solution for the unknown parameter $\boldsymbol{\theta}$ as

$$\begin{aligned}\mathrm{RMSE}(\boldsymbol{\theta}) &= \sqrt{\mathbb{E}\left[\Delta\boldsymbol{\theta}\Delta\boldsymbol{\theta}^T\right]} \\ &= \sqrt{(\boldsymbol{G}^{oT}\boldsymbol{R}^{o-1}\boldsymbol{G}^o)^{-1}}.\end{aligned} \tag{89}$$

By analyzing (89), we find that the theoretical RMSE of the CWLS solution for the unknown parameters increases as the noise covariance $\sigma_{\rho_i}^2$, $\sigma_{d_i}^2$, and $\sigma_{\boldsymbol{q}_i}^2$ (where $i = 1, \ldots, M$) increase.

C. Complexity Analysis

In this section, we analyze the computational complexities of the proposed SDP method and the iterative method in [39] for comparison. The computational complexity of matrix $\boldsymbol{F}$ in (37) can be approximated as $\mathcal{O}(8M^3 + 4M^2(2K+8) + 2M(2K+8)^2)$. It is known that the worst case complexity for solving an SDP problem can be estimated as $\mathcal{O}((p^3 + p^2q^2 + pq^3)q^{0.5})$ defined in [45]. Here, p represents the number of equality constraints in the standard form of the SDP problem and q represents the dimension of the semidefinite cone constraints. For our specific SDP problem in (40), we have $p = 9$ and $q = 2K + 9$. Consequently, the estimated complexity of the SDP-M is roughly $\mathcal{O}(9(2K+9)^{3.5})$. Therefore, the total complexity, accounting for solving the SDP problem twice to obtain the final solution, is approximately $\mathcal{O}(16M^3 + 8M^2(2K+8) + 4M(2K+8)^2 + 18(2K+9)^{3.5})$. In addition, the computational complexity of the iterative method in [39] can be approximated as $\mathcal{O}((8M^2(K+1) + 8M(K+1)^2 + (2K+2)^3 + (2K+2)^2)N)$, where N represents the number of iterations and is related to the accuracy of the initial estimation and the size of the problem. From the above analysis, we can find that the SDP method maintains a constant complexity when the problem size is given, while the complexity of the iterative method increases with the number of iterations N.

V. Numerical Simulation

To evaluate the JLAS performance of the proposed SDP method, numerical simulations are performed in this section. We choose the iterative method (LAS-SDT) discussed in [39] for comparison. We employ the CRLB as a benchmark to assess the accuracy of parameter estimation. In the simulations, we measure the RMSE for the estimated parameters. To illustrate this, we use the position result as an example.

$$\boldsymbol{G}^o = \begin{bmatrix} -2\left(\boldsymbol{q}_1^o - \boldsymbol{p} - \boldsymbol{v}\Delta t_1\right)^T & -2\Delta t_1\left(\boldsymbol{q}_1^o - \boldsymbol{p} - \boldsymbol{v}\Delta t_1\right)^T & 2\left(\rho_1^o - \zeta - \omega\Delta t_1\right) & 2\Delta t_1\left(\rho_1^o - \zeta - \omega\Delta t_1\right) \\ \vdots & \vdots & \vdots & \vdots \\ -2\left(\boldsymbol{q}_M^o - \boldsymbol{p} - \boldsymbol{v}\Delta t_M\right)^T & -2\Delta t_M\left(\boldsymbol{q}_M^o - \boldsymbol{p} - \boldsymbol{v}\Delta t_M\right)^T & 2\left(\rho_M^o - \zeta - \omega\Delta t_M\right) & 2\Delta t_M\left(\rho_M^o - \zeta - \omega\Delta t_M\right) \\ -\boldsymbol{v}^T & \left(\boldsymbol{q}_1^o - \boldsymbol{p} - 2\boldsymbol{v}\Delta t_1\right)^T & -\left(d_1^o - \omega\right) & -\left(\rho_1^o - \zeta - \omega\Delta t_1\right) - \left(d_1^o - \omega\right) \\ \vdots & \vdots & \vdots & \vdots \\ -\boldsymbol{v}^T & \left(\boldsymbol{q}_M^o - \boldsymbol{p} - 2\boldsymbol{v}\Delta t_M\right)^T & -\left(d_M^o - \omega\right) & -\left(\rho_M^o - \zeta - \omega\Delta t_M\right) - \left(d_M^o - \omega\right) \end{bmatrix}_{2M\times(2K+2)} \tag{72}$$

$$\boldsymbol{C}_1^o = \mathrm{diag}\left\{-2\left(\rho_1^o - \zeta - \omega\Delta t_1\right), \ldots, -2\left(\rho_M^o - \zeta - \omega\Delta t_M\right)\right\} \tag{73}$$

$$\boldsymbol{C}_2^o = \mathrm{diag}\left\{\left(d_1^o - \omega\right), \ldots, \left(d_M^o - \omega\right)\right\} \tag{74}$$

$$\boldsymbol{D}_2^o = \mathrm{diag}\left\{\left(\rho_1^o - \zeta - \omega\Delta t_1\right), \ldots, \left(\rho_M^o - \zeta - \omega\Delta t_M\right)\right\} \tag{75}$$

$$\boldsymbol{L}_1^o = \mathrm{diag}\left\{2\left(\boldsymbol{q}_1^{oT} - \boldsymbol{p}^T - \boldsymbol{v}^T\Delta t_1\right), \ldots, 2\left(\boldsymbol{q}_M^{oT} - \boldsymbol{p}^T - \boldsymbol{v}^T\Delta t_M\right)\right\} \tag{76}$$

$$\boldsymbol{L}_2^o = \mathrm{diag}\left\{\left(\boldsymbol{v}^T\right), \ldots, \left(\boldsymbol{v}^T\right)\right\}_{M\times MK} \tag{77}$$

$$\boldsymbol{P}^{o-1} = \begin{bmatrix} -\frac{1}{2}\mathrm{diag}\left\{\frac{1}{\left(\rho_1^o - \zeta - \omega\Delta t_1\right)}, \ldots, \frac{1}{\left(\rho_M^o - \zeta - \omega\Delta t_M\right)}\right\} & \boldsymbol{0}_{M\times M} \\ \frac{1}{2}\mathrm{diag}\left\{\frac{\left(d_1^o - \omega\right)}{\left(\rho_1^o - \zeta - \omega\Delta t_1\right)^2}, \ldots, \frac{\left(d_M^o - \omega\right)}{\left(\rho_M^o - \zeta - \omega\Delta t_M\right)^2}\right\} & \mathrm{diag}\left\{\frac{1}{\left(\rho_1^o - \zeta - \omega\Delta t_1\right)}, \ldots, \frac{1}{\left(\rho_M^o - \zeta - \omega\Delta t_M\right)}\right\} \end{bmatrix}_{2M\times 2M} \tag{78}$$

The RMSE is expressed as

$$\text{RMSE} = \sqrt{\frac{1}{K_1}\sum_{1}^{K_1}\|\boldsymbol{p}-\hat{\boldsymbol{p}}\|^2} \tag{90}$$

where K_1 represents the number of Monte-Carlo runs and $\hat{\boldsymbol{p}}$ is the position result of the proposed method within an individual simulation.

A. Simulation Settings

We establish a 2-D simulation scene that includes eight ANs with the position error located at the corners and midpoints of the sides in a 600 × 600 m square region, as depicted in Fig. 2. Without loss of generality, we consider a single moving UN as an example. UN's position is categorized into two scenarios: the *inside case* and the *outside case*. In the *inside case*, the UN locates randomly at red dots within the convex hull constructed by ANs, as illustrated in the same figure. In the *outside case*, UN's locations are randomly at the black dots outside the convex hull of ANs, as displayed in the same figure. The velocity magnitude of the UN, denoted as $\|\boldsymbol{v}\|$, is randomly sampled from the uniform distribution $\mathcal{U}(0, 50)$ m/s, with its directions drawn from $\mathcal{U}(0, 2\pi)$. At the beginning of each simulation run, we randomly initialize the UN's clock offset and clock drift. The measurement bias caused by the clock offset is generated from a uniform distribution $\mathcal{U}(0, 150)$ m, while the clock drift is derived from $\mathcal{U}(0, 15)$ m/s. The time interval between the consecutive one-way TOA or Doppler shift measurements is fixed at 10 ms. We vary the standard deviation (STD) of the one-way TOA measurement noise σ_ρ from 1 to 10 m, and the STD of the Doppler shift measurement noise σ_d is numerically equal to the one-way TOA measurement noise, but in the unit of m/s. For each noise level, we run 5000 Monte-Carlo simulations.

B. Estimation Performance in Different Scenarios

The estimation performance of the proposed SDP method is influenced by the estimation variance of the unknown parameters, which consist of three fundamental components: measurement errors, AN position errors and the relative geometry between the ANs [46]. To quantify the influence of relative geometry, we use the geometric dilution of precision (GDOP) as a core parameter. The estimation variance of the unknown parameters can be expressed as

$$\begin{aligned}\sigma_\theta^2 &= \text{GDOP}^2 \cdot \left(\sigma_n^2 + K\sigma_{\boldsymbol{q}}^2\right) \\ &= \text{tr}(((\nabla_{\boldsymbol{\theta}}\boldsymbol{\gamma}^o)^T(\nabla_{\boldsymbol{\theta}}\boldsymbol{\gamma}^o))^{-1}) \cdot \left(\sigma_n^2 + K\sigma_{\boldsymbol{q}}^2\right)\end{aligned} \tag{91}$$

where σ_θ^2 is the estimation variance of the unknown parameter, σ_n^2 is the variance of the measurement error, $\sigma_{\boldsymbol{q}}^2$ is the variance of the AN position error, K is the coordinate dimension of the AN, and the GDOP represents the amplification factor of the total Gaussian noise ($\sigma_n^2 + K\sigma_{\boldsymbol{q}}^2$). In this section, the estimation performance of the proposed SDP method will be simulated based on different Gaussian noise.

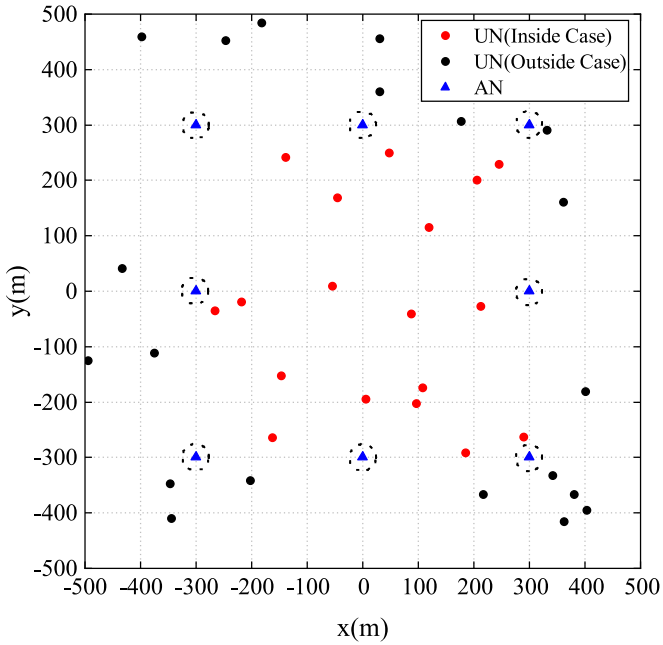

Fig. 2. In this simulation scene, ANs are located at the vertices and midpoints of the edges, and the UN is randomly located at either the red dots (*inside case*) or the black dots (*outside case*). The black dotted circles denote the AN position error.

1) Inside Case: To investigate the estimation performance under varying levels of Gaussian noise, we first held the GDOP constant. According to the contour distribution in Fig. 3, we select the contour with smaller GDOP (GDOP = 1.1321). In this case, the UN is located at [0, 100]. Note that since the UN is moving, the simulated UN's position does not have to be exactly on the GDOP contour line. Then, we study two representative AN position errors: centimeter-level ($\sigma_{\boldsymbol{q}} = 0.01$ m) and decimeter-level ($\sigma_{\boldsymbol{q}} = 0.1$ m).

The estimation results of the proposed SDP method for this case are shown in Figs. 4 and 5, and the results from the iterative method [39] for comparison. It is noteworthy that under the conditions of small Gaussian noise, the estimation accuracy of all parameters for the UN's position, velocity, clock offset, and clock drift reaches the CRLB in the above situation.

2) Outside Case: To further assess the performance of the new SDP method, we investigate its estimation accuracy in another practical scenario, that is, *outside case*. In this case, we also maintain the constant GDOP values and study two representative AN position errors—centimeter-level ($\sigma_{\boldsymbol{q}} = 0.01$ m) and decimeter-level ($\sigma_{\boldsymbol{q}} = 0.1$ m)—to examine the robustness of parameter estimation under varying levels of measurement errors. According to the contour distribution in Fig. 6, we select the contour with larger GDOP (GDOP = 7.72543). In this case, the UN is located at $[-400, 400]$. The estimation results of the proposed SDP method for this case are illustrated in Figs. 7 and 8. The results of the iterative method [39] are accompanied for comparison. The simulation results in Figs. 7 and 8 show that the estimation accuracy of the UN's velocity and clock drift by both methods

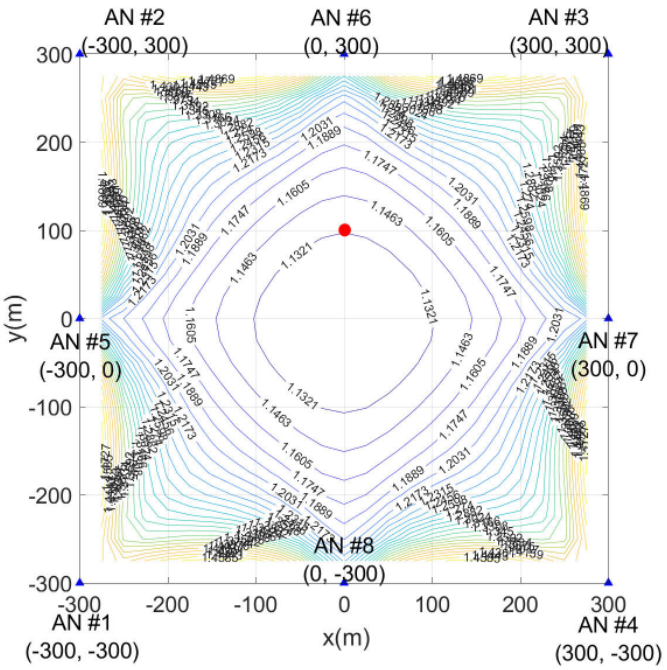

Fig. 3. Contour map of GDOP (*inside case*). According to the contour distribution, we select the contour with a smaller GDOP (GDOP = 1.1321). In this case, the UN is located at [0, 100].

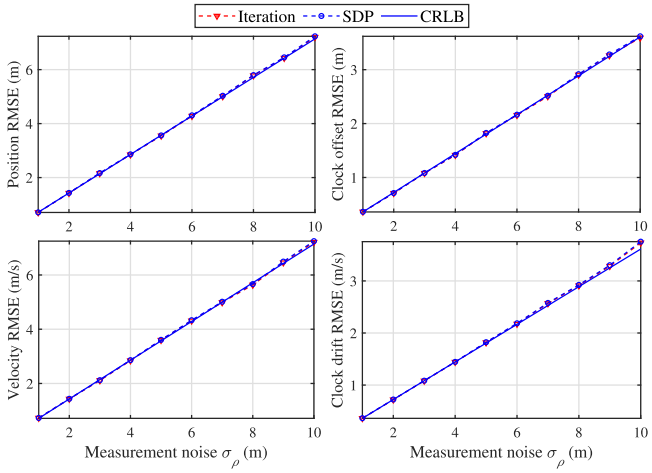

Fig. 4. Estimation RMSEs versus measurement errors with smaller GDOP = 1.1321 (*inside case*) and centimeter-level AN position error (σ_q = 0.01 m). The estimation accuracy of the proposed SDP method reaches the CRLB in the small Gaussian noise.

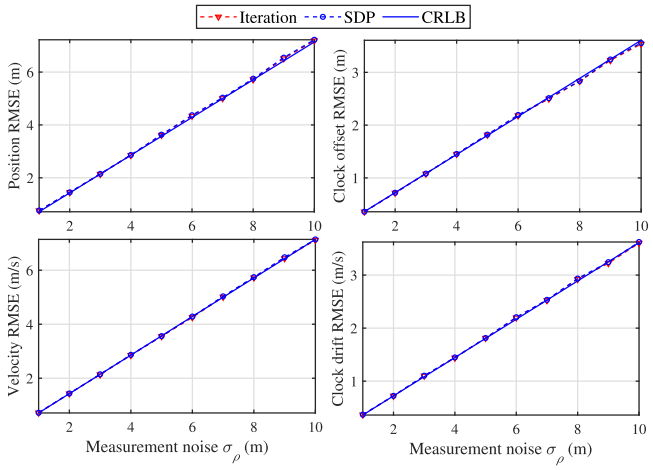

Fig. 5. Estimation RMSEs versus measurement errors with smaller GDOP = 1.1321 (*inside case*) and decimeter-level AN position error (σ_q = 0.1 m). The estimation accuracy of the proposed SDP method reaches the CRLB in the small Gaussian noise.

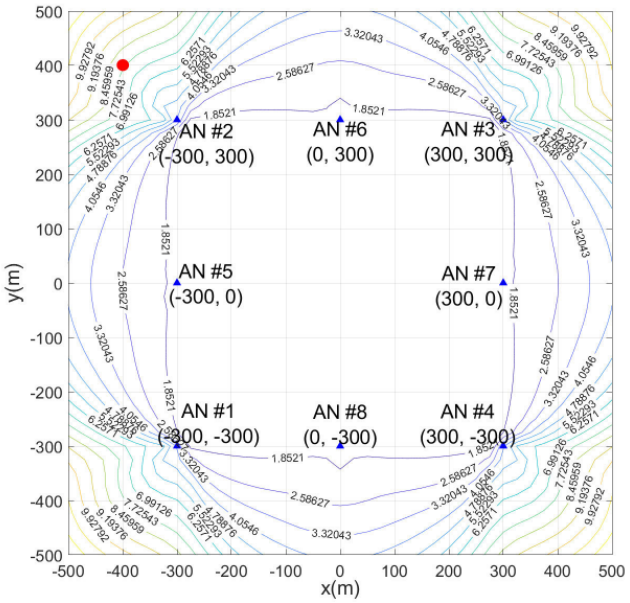

Fig. 6. Contour map of GDOP (*outside case*). According to the contour distribution, we select the contour with a larger GDOP (GDOP = 7.72543). In this case, the UN is located at [−400, 400].

reaches the CRLB in the small Gaussian noise and the estimation accuracy for the UN's position and clock offset, in both methods, deviates from the CRLB. This deviation is due to the large GDOP (GDOP = 7.72543) in this situation, the amplification factor for the same Gaussian noise is roughly seven times that of the case in Figs. 4 and 5 with GDOP = 1.1321. In addition, in Figs. 7 and 8, compared with the iterative method, the estimation accuracy of the SDP method for the UN's position and clock offset deviates more from the CRLB. It shows that the proposed SDP method is more sensitive to the GDOP than the iterative method. In the future, we will try to explore and add new constraints to tighten the current SDP problem and improve its robustness to the ANs' relative geometry, so that good estimate results can be obtained under poor GDOP conditions, such as GDOP > 7 in the scenario of Fig. 6.

C. Comparison with the Iterative Method

To compare the robustness of both methods, we assess the position RMSE of the two methods given different initial positions $\boldsymbol{p}_0$. These initial positions are set at different circumference radii: 10, 60, 100, 150, and 200 m, all centered at the true position, representing an initial estimate that deviates from the true position. The UN is located at [0, 0] and AN position error STD σ_q sets as 0.01 m for this simulation. We run 5000 Monte-Carlo simulations for each measurement error while keeping other settings unchanged.

TABLE I
NUMBER OF RESULTS FOR ALL CASES OF THE ITERATION METHOD WITH DIFFERENT INITIAL POSITION ERROR

	Initial Position Error (m)	10	60	100	150	200
(a)	Correct Estimate ($error < 3\sqrt{CRLB}$)	4999	4999	4999	4974	4810
(b)	Convergence ($increment\ norm < 0.01m$)	5000	5000	5000	4971	4793
(c)	Number of Iterations Exceed ($iter \geq 10$)	0	0	0	13	77

Note: The measurement error is $\sigma_\rho = 5$ m. As the initial position errors increase, the number of results in cases (a) and (b) decreases, while the number of results in cases (c) increases. This indicates that the estimation performance of the iterative method strongly depends on the accuracy of the initial position value.

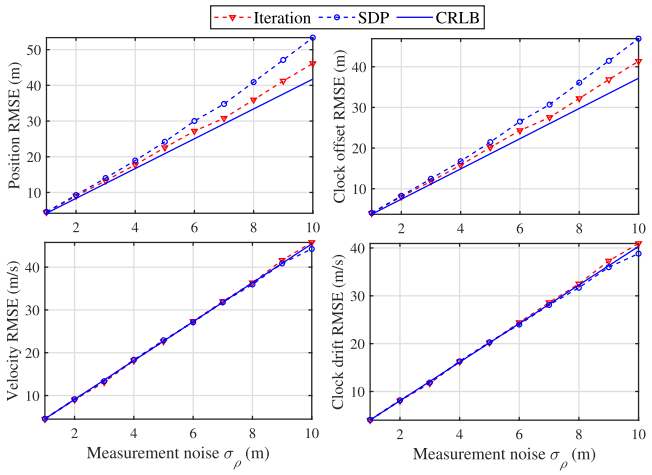

Fig. 7. Estimation RMSEs versus measurement errors with larger GDOP = 7.72543 (*outside case*) and centimeter-level AN position error (σ_q = 0.01 m). The estimation accuracy of the proposed SDP method for the position and clock offset deviates from CRLB due to the large GDOP, which amplifies the Gaussian noise by about seven times compared to Fig. 4.

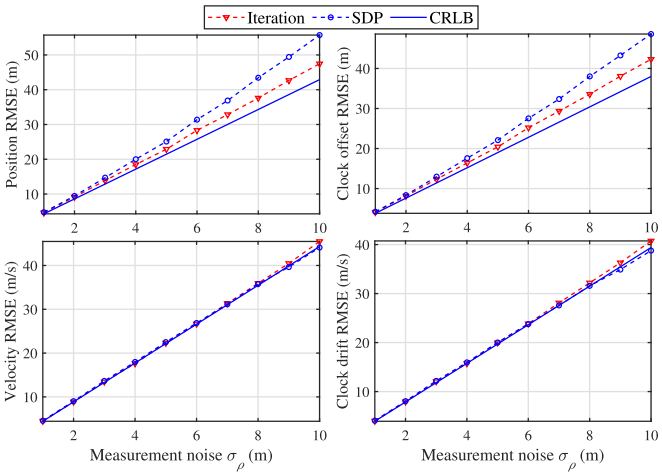

Fig. 8. Estimation RMSEs versus measurement errors with larger GDOP = 7.72543 (*outside case*) and decimeter-level AN position error (σ_q = 0.1 m). The estimation accuracy of the proposed SDP method for the position and clock offset deviates from CRLB due to the large GDOP, which amplifies the Gaussian noise by about seven times compared to Fig. 5.

For the iterative method [39], we establish two criteria to terminate the iteration.

1) *Convergence:* The norm of the parameter estimate increment in the current iteration is defined as *increment norm*. If the *increment norm* is smaller than $thr = 0.01$ m, the iterative method is terminated.
2) *Number of Iterations Exceeded:* If the number of iterations surpasses 10, the iterative method is terminated.

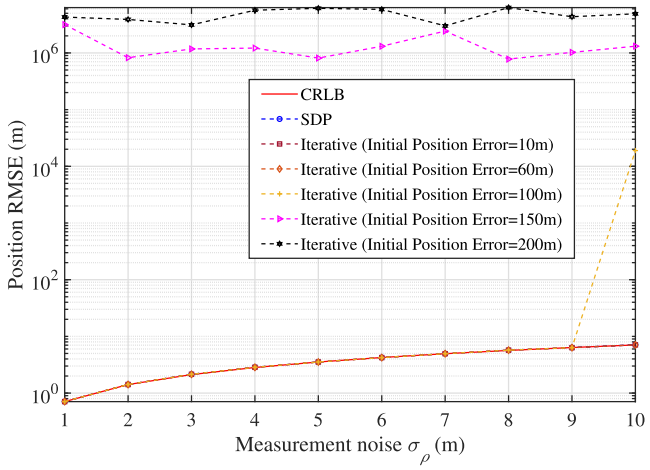

Fig. 9. Position RMSE versus measurement errors (GDOP = 1.1179 and σ_q = 0.01 m). The position RMSE for the iterative method is only calculated in the convergence case. We can observe that when the initial position error is large, the RMSE of the iterative method is significantly larger than SDP-M. Further details on the simulation results for $\sigma_\rho = 5$ m can be found in Table I.

Furthermore, we introduce a uniform threshold, denoted as $3\sqrt{\text{CRLB}}$, to determine the correctness of results, indicated as *correct estimate*. We only display the position RMSE for the *convergence* case in Fig. 9. As shown in Fig. 9, the position estimation accuracy of the proposed SDP method aligns closely with the CRLB. However, the performance of the iterative method varies with the initial position accuracy. Notably, when the initial position error circumferential radius (10 and 60 m) of the iterative method is small, the position estimation accuracy consistently reaches the CRLB. Conversely, for larger initial position error circumferential radii (100, 150, and 200 m), the position estimation accuracy deviates from the CRLB even if the iterative method converges.

We closely examine the results of the iterative method in Fig. 9 and the number of simulation results for the $\sigma_\rho = 5$ m case are listed in Table I. As the table shows, as the initial position errors increase, the starting point of the iterative method in the parameter space moves further away from the true value. This causes the iterative method to encounter issues like local minima or nonconvergence, leading to a decrease in the counts for both correct estimate and the convergence

cases. Furthermore, larger initial position errors significantly increase the number of iterations required to approximate the target solution. Additionally, during each iteration, the cumulative effect of the initial position errors propagates estimation inaccuracies, making subsequent iterations increasingly complex and unstable, which ultimately increases the counts of the number of iterations exceeded. This table highlights the pivotal role of proper initialization in the iterative method. The bias of the final estimate in the iterative method is significantly affected by the inaccurate initial UN's position.

VI. Conclusion

In this article, we propose a novel SDP method to address the JLAS problem for the moving UNs with the clock offset and the clock drift in a TDBLAS system with the AN position error. In this method, we first introduce the optimization variable and formulate a CWLS problem using the sequential one-way TOA and Doppler shift measurements, which are high-dimensional nonlinear and nonconvex. Then, we propose a novel SDR method, which efficiently relaxes the complex and nonconvex CWLS problem into a convex and tractable SDP problem. Compared to the conventional iterative method [39], which usually suffers from the local minima or nonconvergence without an accurate initial guess, the proposed SDP method can guarantee the global optimum without the initialization under small Gaussian noise.

Theoretical analysis of the estimation error shows that the CWLS solution reaches the CRLB under small Gaussian noise. Numerical results reveal that the proposed SDP method reaches the CRLB under small Gaussian noise. In addition, the novel SDP method is more robust and always obtains the global optimal solution without precise initialization under small Gaussian noise compared to the conventional iterative method [39].

References

[1] S. Kuutti, S. Fallah, K. Katsaros, M. Dianati, F. Mccullough, and A. Mouzakitis, "A survey of the state-of-the-art localization techniques and their potentials for autonomous vehicle applications," *IEEE Internet Things J.*, vol. 5, no. 2, pp. 829–846, Apr. 2018.

[2] F. Yang, S. Wang, J. Li, Z. Liu, and Q. Sun, "An overview of Internet of Vehicles," *China Commun.*, vol. 11, no. 10, pp. 1–15, Oct. 2014.

[3] A. F. G. G. Ferreira, D. M. A. Fernandes, A. P. Catarino, and J. L. Monteiro, "Localization and positioning systems for emergency responders: A survey," *IEEE Commun. Surveys Tuts.*, vol. 19, no. 4, pp. 2836–2870, 4th Quart., 2017.

[4] R. W. Beard, T. W. McLain, M. A. Goodrich, and E. P. Anderson, "Coordinated target assignment and intercept for unmanned air vehicles," *IEEE Trans. Robot. Autom.*, vol. 18, no. 6, pp. 911–922, Dec. 2002.

[5] I. Guvenc and C.-C. Chong, "A survey on TOA based wireless localization and NLOS mitigation techniques," *IEEE Commun. Surveys Tuts.*, vol. 11, no. 3, pp. 107–124, 3rd Quart., 2009.

[6] Y. Wang, S. Ma, and C. L. P. Chen, "TOA-based passive localization in quasi-synchronous networks," *IEEE Commun. Lett.*, vol. 18, no. 4, pp. 592–595, Apr. 2014.

[7] S. Wu, S. Zhang, and D. Huang, "A TOA-based localization algorithm with simultaneous NLOS mitigation and synchronization error elimination," *IEEE Sensors Lett.*, vol. 3, no. 3, pp. 1–4, Mar. 2019.

[8] T. Qiao, Y. Zhang, and H. Liu, "Nonlinear expectation maximization estimator for TDOA localization," *IEEE Wireless Commun. Lett.*, vol. 3, no. 6, pp. 637–640, Dec. 2014.

[9] X. Qu and L. Xie, "An efficient convex constrained weighted least squares source localization algorithm based on TDOA measurements," *Signal Process.*, vol. 119, pp. 142–152, Feb. 2016.

[10] H.-J. Shao, X.-P. Zhang, and Z. Wang, "Efficient closed-form algorithms for AOA based self-localization of sensor nodes using auxiliary variables," *IEEE Trans. Signal Process.*, vol. 62, no. 10, pp. 2580–2594, May 2014.

[11] S. Tomic, M. Beko, and R. Dinis, "3-D target localization in wireless sensor networks using RSS and AoA measurements," *IEEE Trans. Veh. Technol.*, vol. 66, no. 4, pp. 3197–3210, Apr. 2017.

[12] S. Zhao, X.-P. Zhang, X. Cui, and M. Lu, "Semidefinite programming two-way TOA localization for user devices with motion and clock drift," *IEEE Signal Process. Lett.*, vol. 28, pp. 578–582, 2021.

[13] N. Guo, S. Zhao, X.-P. Zhang, Z. Yao, X. Cui, and M. Lu, "New closed-form joint localization and synchronization using sequential one-way TOAs," *IEEE Trans. Signal Process.*, vol. 70, pp. 2078–2092, Apr. 2022.

[14] J.-A. Luo, X.-P. Zhang, and Z. Wang, "A new passive source localization method using AOA-GROA-TDOA in wireless sensor array networks and its Cramér-rao bound analysis," in *Proc. IEEE Int. Conf. Acoust., Speech Signal Process.*, May 2013, pp. 4031–4035.

[15] Q. Wei, X. Chen, C. Jiang, and Z. Huang, "Time-of-arrival estimation for integrated satellite navigation and communication signals," *IEEE Trans. Wireless Commun.*, vol. 22, no. 12, pp. 9867–9880, Dec. 2023.

[16] B. Denis, J.-B. Pierrot, and C. Abou-Rjeily, "Joint distributed synchronization and positioning in UWB ad hoc networks using TOA," *IEEE Trans. Microw. Theory Techn.*, vol. 54, no. 4, pp. 1896–1911, Jun. 2006.

[17] R. M. Vaghefi and R. M. Buehrer, "Cooperative joint synchronization and localization in wireless sensor networks," *IEEE Trans. Signal Process.*, vol. 63, no. 14, pp. 3615–3627, Jul. 2015.

[18] A. Ahmad, E. Serpedin, H. Nounou, and M. Nounou, "Joint node localization and time-varying clock synchronization in wireless sensor networks," *IEEE Trans. Wireless Commun.*, vol. 12, no. 10, pp. 5322–5333, Oct. 2013.

[19] J. Zheng and Y.-C. Wu, "Joint time synchronization and localization of an unknown node in wireless sensor networks," *IEEE Trans. Signal Process.*, vol. 58, no. 3, pp. 1309–1320, Mar. 2010.

[20] F. Zafari, A. Gkelias, and K. K. Leung, "A survey of indoor localization systems and technologies," *IEEE Commun. Surveys Tuts.*, vol. 21, no. 3, pp. 2568–2599, 3rd Quart., 2019.

[21] S. Zhao, X. Cui, F. Guan, and M. Lu, "A Kalman filter-based short baseline RTK algorithm for single-frequency combination of GPS and BDS," *Sensors*, vol. 14, no. 8, pp. 15415–15433, Aug. 2014.

[22] T. Jia, K. C. Ho, H. Wang, and X. Shen, "Localization of a moving object with sensors in motion by time delays and Doppler shifts," *IEEE Trans. Signal Process.*, vol. 68, pp. 5824–5841, 2020.

[23] G. Wang, S. Cai, Y. Li, and N. Ansari, "A bias-reduced nonlinear WLS method for TDOA/FDOA-based source localization," *IEEE Trans. Veh. Technol.*, vol. 65, no. 10, pp. 8603–8615, Oct. 2016.

[24] L. Yang, L. Yang, and K. C. Ho, "Moving target localization in multistatic sonar by differential delays and Doppler shifts," *IEEE Signal Process. Lett.*, vol. 23, no. 9, pp. 1160–1164, Sep. 2016.

[25] H.-W. Wei, R. Peng, Q. Wan, Z.-X. Chen, and S.-F. Ye, "Multidimensional scaling analysis for passive moving target localization with TDOA and FDOA measurements," *IEEE Trans. Signal Process.*, vol. 58, no. 3, pp. 1677–1688, Mar. 2010.

[26] G. Wang, R. Zheng, and K. C. Ho, "Elliptic localization of a moving object by transmitter at unknown position and velocity: A semidefinite relaxation approach," *IEEE Trans. Mobile Comput.*, vol. 22, no. 5, pp. 2675–2692, May 2023.

[27] Q. Shi, X. Cui, S. Zhao, S. Xu, and M. Lu, "BLAS: Broadcast relative localization and clock synchronization for dynamic dense multiagent systems," *IEEE Trans. Aerosp. Electron. Syst.*, vol. 56, no. 5, pp. 3822–3839, Oct. 2020.

[28] S. Zhao, X.-P. Zhang, X. Cui, and M. Lu, "Optimal localization with sequential pseudorange measurements for moving users in a time-division broadcast positioning system," *IEEE Internet Things J.*, vol. 8, no. 11, pp. 8883–8896, Jun. 2021.

[29] Q. Shi, X. Cui, S. Zhao, and M. Lu, "Sequential TOA-based moving target localization in multi-agent networks," *IEEE Commun. Lett.*, vol. 24, no. 8, pp. 1719–1723, Aug. 2020.

[30] B. Hofmann-Wellenhof, H. Lichtenegger, and E. Wasle, *GNSS–global Navigation Satellite Systems: GPS, GLONASS, Galileo, and More*. Cham, Switzerland: Springer, 2007.

[31] A. V. Picois and N. Samama, "Near-far interference mitigation for pseudolites using double transmission," *IEEE Trans. Aerosp. Electron. Syst.*, vol. 50, no. 4, pp. 2929–2941, Oct. 2014.

[32] P. Misraand and P. K. Enge, "The global positioning system: Signals, measurements, and performance," *Int. J. Wireless Inf. Netw.*, vol. 1, no. 2, pp. 83–105, Apr. 2010.
[33] H. G. Myung, J. Lim, and D. J. Goodman, "Single carrier FDMA for uplink wireless transmission," *IEEE Veh. Technol. Mag.*, vol. 1, no. 3, pp. 30–38, Sep. 2006.
[34] S. Zhao, N. Guo, X.-P. Zhang, X. Cui, and M. Lu, "Closed-form two-way TOA localization and synchronization for user devices with motion and clock drift," *IEEE Signal Process. Lett.*, vol. 29, pp. 100–104, 2022.
[35] S. Dwivedi, D. Zachariah, A. De Angelis, and P. Handel, "Cooperative decentralized localization using scheduled wireless transmissions," *IEEE Commun. Lett.*, vol. 17, no. 6, pp. 1240–1243, Jun. 2013.
[36] D. Zachariah, A. Angelis, S. Dwivedi, and P. Händel, "Self-localization of asynchronous wireless nodes with parameter uncertainties," *IEEE Signal Process. Lett.*, vol. 20, no. 6, pp. 551–554, Jun. 2013.
[37] P. Carroll, S. Zhou, K. Mahmood, H. Zhou, X. Xu, and J. Cui, "On-demand asynchronous localization for underwater sensor networks," *IEEE Trans. Signal Process.*, vol. 62, no. 13, pp. 3337–3348, Jul. 2014.
[38] J. Yan, X. Zhang, X. Luo, Y. Wang, C. Chen, and X. Guan, "Asynchronous localization with mobility prediction for underwater acoustic sensor networks," *IEEE Trans. Veh. Technol.*, vol. 67, no. 3, pp. 2543–2556, Mar. 2018.
[39] S. Zhao, N. Guo, X.-P. Zhang, X. Cui, and M. Lu, "Sequential Doppler-shift-based optimal localization and synchronization with TOA," *IEEE Internet Things J.*, vol. 9, no. 17, pp. 16234–16246, Sep. 2022.
[40] T. Jia, X. Ke, H. Liu, K. C. Ho, and H. Su, "Target localization and sensor self-calibration of position and synchronization by range and angle measurements," *IEEE Trans. Signal Process.*, vol. 73, pp. 340–355, 2025.
[41] Y. Zou and H. Liu, "Semidefinite programming methods for alleviating clock synchronization bias and sensor position errors in TDOA localization," *IEEE Signal Process. Lett.*, vol. 27, pp. 241–245, 2020.
[42] Y. Wang and K. C. Ho, "TDOA source localization in the presence of synchronization clock bias and sensor position errors," *IEEE Trans. Signal Process.*, vol. 61, no. 18, pp. 4532–4544, Sep. 2013.
[43] B. Ren, T. Jia, H. Liu, Y. Wang, and J. Yan, "Efficient estimation for sensor biases and target states in the presence of sensor position errors," *IEEE Sensors J.*, vol. 24, no. 10, pp. 16551–16562, May 2024.
[44] S. M. Kay, *Fundamentals of Statistical Signal Processing: Estimation Theory*. Upper Saddle River, NJ, USA: Prentice-Hall, 1993.
[45] K. Fujisawa, M. Kojima, and K. Nakata, "Exploiting sparsity in primal-dual interior-point methods for semidefinite programming," *Math. Program.*, vol. 79, nos. 1–3, pp. 235–253, Oct. 1997.
[46] E. D. Kaplan and C. Hegarty, *Understanding GPS/GNSS: Principles and Applications*. Norwood, MA, USA: Artech House, 2017.

Yanyan Peng received the B.S. degree in communication engineering from the Civil Aviation University of China, Tianjin, China, in 2021. She is currently pursuing the Ph.D. degree with Beijing University of Posts and Telecommunications, Beijing, China.

Her current research interests include signal processing, localization, and optimization methods.

Ningyan Guo received the Ph.D. degree in instrument science and optoelectronics engineering from Beihang University, Beijing, China, in 2014.

From 2010 to 2012, she was a Visiting Scholar at the Department of Aerospace Engineering Sciences, University of Colorado Boulder, Boulder, CO, USA. From 2014 to 2019, she was a Communication Systems Engineer at Beijing Research Institute of Mechanical and Electrical Technology, Beijing. From 2019 to 2021, she was a Postdoctoral Researcher with the Department of Electronic Engineering, Tsinghua University, Beijing. Since 2022, she has been an Associate Professor with the School of Information and Communication Engineering, Beijing University of Posts and Telecommunications, Beijing. Her current research interests include localization algorithms, high-precision positioning techniques, and integrated positioning and communication.

Sihao Zhao (Senior Member, IEEE) received the B.S. and Ph.D. degrees in electronic engineering from Tsinghua University, Beijing, China, in 2005 and 2011, respectively.

He is currently a Senior Algorithm Designer with NovAtel, Autonomy and Positioning Division of Hexagon, Calgary, AB, Canada. From 2011 to 2013, he was an Electronics Systems Engineer with China Academy of Space Technology, Beijing. From 2013 to 2019, he was a Postdoctoral Researcher and an Assistant Professor with the Department of Electronic Engineering, Tsinghua University. From 2020 to 2021, he was a Research Associate with the Department of Electrical, Computer and Biomedical Engineering, Toronto Metropolitan University, Toronto, ON, Canada. His research interests include localization algorithms, high-precision positioning techniques, and indoor navigation system development.

Dr. Zhao is an Editor of GPS Solutions.

Chunxiao Jiang (Fellow, IEEE) received the B.S. (Hons.) degree in information engineering from Beihang University, Beijing, China, in 2008, and the Ph.D. (Hons.) degree in electronic engineering from Tsinghua University, Beijing, in 2013.

He was with the Department of Electrical and Computer Engineering, University of Maryland College Park, College Park, MD, USA, under the supervision of Prof. K. J. Ray Liu, as a Joint Ph.D. Student, from 2011 to 2012 and a Postdoctoral Researcher, from 2013 to 2016. He is an Associate Professor at the School of Information Science and Technology, Tsinghua University. His research interests include the application of game theory, optimization, and statistical theories to communication, networking, and resource allocation problems, in particular, space networks and heterogeneous networks.

Dr. Jiang is a Fellow of IET. He served as a member of the Technical Program Committee as well as the symposium chair for a number of international conferences. He was a recipient of the Best Paper Award from the IEEE GLOBECOM in 2013, the IEEE Communications Society Young Author Best Paper Award in 2017, the Best Paper Award from the ICC in 2019, the IEEE VTS Early Career Award 2020, the IEEE ComSoc Asia–Pacific Best Young Researcher Award 2020, the IEEE VTS Distinguished Lecturer 2021, and the IEEE ComSoc Best Young Professional Award in Academia 2021. He received the Chinese National Second Prize in Technical Inventions Award in 2018 and the Natural Science Foundation of China Excellent Young Scientists Fund Award in 2019. He served as an Editor for IEEE TRANSACTIONS ON COMMUNICATIONS, IEEE INTERNET OF THINGS JOURNAL, IEEE WIRELESS COMMUNICATIONS, IEEE TRANSACTIONS ON NETWORK SCIENCE AND ENGINEERING, IEEE NETWORK, and IEEE COMMUNICATIONS LETTERS, and a Guest Editor for *IEEE Communications Magazine*, IEEE TRANSACTIONS ON NETWORK SCIENCE AND ENGINEERING, and IEEE TRANSACTIONS ON COGNITIVE COMMUNICATIONS AND NETWORKING.

Zhiyong Feng (Senior Member, IEEE) received the B.S., M.S., and Ph.D. degrees in information and communication engineering from Beijing University of Posts and Telecommunications (BUPT), Beijing, China, in 1993, 1997, and 2009, respectively.

She is the Director of the Key Laboratory, Universal Wireless Communications, Ministry of Education, Beijing. She is a Technical Advisor of NGMN. Her main research interests include wireless network architecture design and radio resource management in 5th-generation mobile networks (5G), spectrum sensing and dynamic spectrum management in cognitive wireless networks, universal signal detection and identification, and network information theory.

Dr. Feng is an Editor of IET Communications and KSII Transactions on Internet and Information Systems, and a reviewer of IEEE TRANSACTIONS ON WIRELESS COMMUNICATIONS, IEEE TRANSACTIONS ON VEHICULAR TECHNOLOGY, and IEEE JOURNAL ON SELECTED AREAS IN COMMUNICATIONS. She is active in ITU-R, IEEE, ETSI, and CCSA standards.